Int J Earth Sci (Geol Rundsch) (2010) 99:1859–1886
DOI 10.1007/s00531-009-0475-8

ORIGINAL PAPER

# Integrated stratigraphy and $^{40}Ar/^{39}Ar$ chronology of the early to middle Miocene Upper Freshwater Molasse in western Bavaria (Germany)

**Hayfaa Abdul Aziz · Madelaine Böhme · Alexander Rocholl · Jerome Prieto · Jan R. Wijbrans · Valerian Bachtadse · Albert Ulbig**

Received: 30 September 2008 / Accepted: 7 July 2009 / Published online: 11 August 2009


**Abstract** A detailed integrated stratigraphic study (biostratigraphy and magnetostratigraphy) was carried out on five sections from the western part of the Bavarian Upper Freshwater Molasse of the North Alpine Foreland Basin (NAFB), greatly improving the chronostratigraphy of these sediments. The sections belong to the lithostratigraphic units *Limnische Untere Serie* (UL) and *Fluviatile Untere Serie* (UF) and contain 19 (mostly new) small-mammal bearing levels, significantly refining the local biostratigraphy. Radiometric ages obtained from glass shards from tuff horizons are used together with the biostratigraphic information for constructing and confirming the magnetostratigraphic correlation of the studied sections to the Astronomical Tuned Time Scale (ANTS04; Lourens et al. in Geologic Time Scale 2004, Cambridge University Press, 2004). This correlation implies that the UL lithostratigraphic unit corresponds to the latest Ottnangian and the Early Karpatian, whereas the UF corresponds to the Karpatian and the Early Badenian. This indicates that the Brackish- to Freshwater Molasse transition already occurred during the late Ottnangian. The pre-Riesian hiatus occurred in the latest Karpatian and lower Early Badenian in Eastern Bavaria and Bohemia and in the Late Karpatian and earliest Badenian in Western Bavaria. The geochemical and Ar–Ar data of volcanic ashes suggest that highly evolved silicic magmas from a single volcano or volcanic center, characterized by a uniform Nd isotopic composition, erupted repetitively over the course of at least 1.6 Myr. Three phases of eruptive activity were identified at 16.1 ± 0.2 Ma (Zahling-2), 15.6 ± 0.4 Ma (Krumbad), and 14.5 ± 0.2 Ma (Heilsberg, Hegau). The correlation of the local biostratigraphic zonation to the ANTS04 enables further the characterization of both the Ottnangian–Karpatian and Karpatian–Badenian boundaries in the NAFB by small-mammal biostratigraphy. According to these results the Ottnangian–Karpatian boundary is contemporaneous with the first appearance datum of *Megacricetodon bavaricus* (in the size of the type population) and the first common occurrence of *Keramidomys thaleri*, whereas *Ligerimys florancei*, *Melissiodon dominans* and *Prodeinotherium* aff. *bavaricum* have been already disappeared during the late Ottnangian. The Karpatian–Badenian boundary is characterized by a significant size increase of the large *Megacricetodon* lineage and possibly a (re-)immigration of *Prodeinotherium bavaricum*.

**Keywords** Biostratigraphy · Magnetostratigraphy · $^{40}Ar/^{39}Ar$ dating · Miocene · Molasse

H. A. Aziz · V. Bachtadse
Department for Earth and Environmental Sciences, Section Geophysics, Ludwig-Maximilians-University Munich, Theresienstrasse 41, 80333 Munich, Germany

M. Böhme (✉) · J. Prieto
Department for Earth and Environmental Sciences, Section Palaeontology, Ludwig-Maximilians-University Munich, Richard-Wagner-Str. 10, 80333 Munich, Germany
e-mail: m.boehme@lrz.uni-muenchen.de

A. Rocholl
Department for Earth and Environmental Sciences, Section Mineralogy, Ludwig-Maximilians-University Munich, Theresienstrasse 41, 80333 Munich, Germany

J. R. Wijbrans
Department of Isotope Geochemistry, Vrije Universiteit Amsterdam, De Boelelaan 1085, 1081 HV Amsterdam, The Netherlands

A. Ulbig
Schlagmann Baustoffe, Ziegeleistrasse 1, 84367 Zeilarn, Germany

## Introduction

The Molasse Basin, also known as the Northern Alpine Foreland Basin (NAFB), is a classical foreland basin situated at the northern margin of the Alps and has been the subject of numerous studies focusing on facies distribution, stratigraphic, sedimentological, and structural evolution of the basin and its response to the tectonic history of the orogenic wedge (Schlunegger et al. 2002; Kuhlemann et al. 2002; Kuhlemann and Kempf 2002, and references therein). More recent studies focus on the role of tectonics and climate on sediment discharge of the Alps to the NAFB, requiring detailed stratigraphic analysis of the basin sedimentary infill and, most importantly, an accurate temporal resolution. In the Swiss part of the Molasse basin, a magneto- and biostratigraphic framework for Oligocene to Middle Miocene sequences has been successfully established (Schlunegger et al. 1996; Kempf et al. 1997, 1999). Conversely, the chronostratigraphy of terrestrial sediments of the Molasse basin in southern Germany (Bavaria), which is one of the richest paleontological and -botanical Neogene basins of Europe, relies beside otolith and charophyte stratigraphy (Reichenbacher 1999; Berger 1999) on (micro)-mammal biostratigraphy combined with lithostratigraphic correlations and sparse radioisotopic datings only (Heissig 1997; Böhme et al. 2002). Since lithostratigraphy depends on facies distribution, it does not provide the temporal resolution necessary for establishing basin-wide stratigraphic correlations. A significant progress was made by Abdul Aziz et al. (2008) due to the establishment of a chronostratigraphy for the Upper Freshwater Molasse in the eastern part of the Molasse Basin (Lower Bavaria) using an integrated approach with biostratigraphy, magnetostratigraphy, and Ar–Ar dating.

Here, we present the results of detailed biostratigraphy and magnetostratigraphy studies together with radioisotopic dating of bentonite marker beds for the Early and Middle Miocene Upper Freshwater Molasse of the western Bavarian part of the Molasse Basin.

## Geological setting and local stratigraphy

The NAFB extends about 1,000 km along the Alpine front from Lake Geneva in the West to the eastern

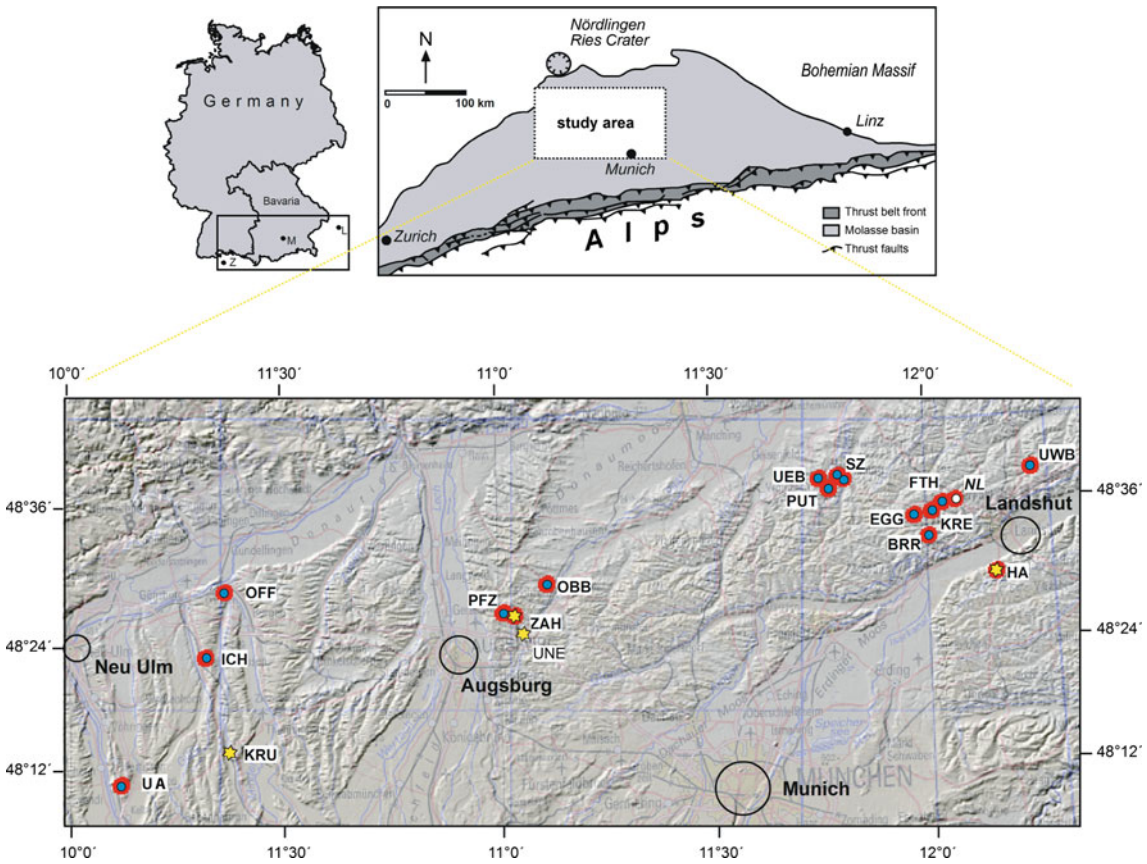


**Fig. 1** Location maps of study area, sections and bentonites, and sketch map of the Molasse Basin. Abbreviations: *KRU* Krumbad bentonite, *ZAH* Zahling-2 glass-tuff, *HA* Hachelstuhl bentonite, *UNE* Unterneul bentonite (the Heilsberg, Hegau bentonite is outside the map). For the abbreviations of sections see Fig. 2

termination of the Alps in Austria (Fig. 1). During the Cenozoic, the NAFB formed as a mechanical response to the tectonic load of the evolving Alps (e.g., Homewood et al. 1986; Schlunegger et al. 1997) causing a flexural bulge in the European lithosphere, which acted as a sediment sink for the erosional debris of the uplifting Alps.

Following the Upper Brackishwater Molasse (=Kirchberg Formation) the Upper Freshwater Molasse (OSM) sedimentary environment is characterized by a pronounced temporal and lateral variability of continental facies. During OSM deposition, radial alluvial fan sedimentation dominated in the southern part of the basin while E–W fluvial–alluvial sedimentation prevailed in the northern part along the basin axis. As a consequence, the OSM is divided into several lithostratgraphic units, which differ significantly from east to west. Since our study area is limited to Bavaria, we only discuss the relevant local lithostratigraphic units (for details see e.g., Doppler 1989, Doppler et al. 2005).

The eastern part of the OSM in the Bavarian Molasse is dominated by the *Nördlicher Vollschotter* (NV; Wurm 1937), a 100 to 200 m thick gravelly lithostratigraphic unit, which is split into two parts by the *Süßwasserkalk* (SK), up to 10 m thick calcareous paleosol horizon (Batsche 1957). The lower part of the NV consists of poorly sorted coarse-grained gravels while the upper part is less coarse and, in the study area, comprises several paleosol horizons. The stratigraphically uppermost paleosol corresponds to the ~7 m thick *Zwischenmergel* (ZM; Hofmann 1973), which is overlain by a gravel unit containing Jurassic limestone boulders of the Ries impact; i.e., the Brock-horizon. Finally, the uppermost gravel-horizon of the NV is overlain by 5–7 m thick fine-grained, marly sediments of the *Sand–Mergel–Decke* (SMD), which includes up to 3 m thick tuff horizon, the so-called main bentonite layer.

The western part of the OSM in the Bavarian Molasse is divided into the lithostratigraphic units *Limnische Untere Serie (UL)* and *Fluviatile Untere Serie (UF)*. The UL, which is considered to be the western equivalent of the oldest part of the NV, is not strictly lacustrine and also includes fluvial-floodplain deposits (Doppler 1989; Doppler et al. 2005). The UL sediments are dominated by gray, sometimes greenish to yellowish, fine sands and (marly) silts and muds and the total thickness is estimated between 60 and 80 m. The younger UF lithostratigraphic unit conformably overlies the UL. The UF sedimentary sequence is about 150 m thick and is laterally equivalent to the main part of the lower NV. The basal part of the UF comprises greenish-gray fine sands, silts, and muds while the upper part typically consists of silts and fine to medium-grained sands (Fig. 2).

*Biozonations*

The Upper Freshwater Molasse is divided on the basis of deinotheriid proboscidians (Dehm 1951, 1955) into an Older Series (without dinotheriids), a Middle Series (with *Prodeinotherium bavaricum*), and a Younger Series (with *Deinotherium* aff. *giganteum*). The Older Series was preceded by a period where *P. bavaricum* was already present (Dehm 1951). These older deinotheriid localities belong or correlate to the Brackish Water Molasse (Hoisberg, Grimm 1957; Langenau; Heizmann 1984), Grimmelfingen beds (Jungnau, Dehm 1951; Eggingen-Mittelhardt, Heizmann 1984; Reichenbacher et al. 1998) and the Upper Marine Molasse (Baltringen, Dehm 1951). The latter locality corresponds to the base of the middle Ottnangian regional stage (Pippèrr et al. 2007) and represents the first appearance datum (FAD) for deinotheriids in the Molasse Basin. The Older Series correspond to the Karpatian regional stage, the Middle Series to the Early Badenian regional stage (Abdul Aziz et al. 2008), whereas the Younger Series correspond probably to the Late Badenian to earliest Pannonian regional stages. The Brackish Water Molasse (including their freshwater equivalents) and the Older and the Middle Series can be subdivided into OSM units on the basis of small-mammals (Heissig 1997; Abdul Aziz et al. 2008). Most important are evolutionary lineages of the cricetid genera *Megacricetodon* and *Cricetodon*, characterized by minor morphological change but significant molar size increase (Fig. 3). The Brackish Water Molasse and the base of the Upper Freshwater Molasse belong to the unit OSM A, which is characterized by *M.* aff. *collongensis.* The Older Series comprise the OSM units B and C + D. The OSM B unit is characterized by *M. bavaricus*, and OSM C + D by *M.* aff. *bavaricus*. In the late part of OSM C + D, a second, smaller sized, *Megacricetodon* species appears (*M.* cf. *minor*). The Middle Series consist of the units OSM E, E′, F, and ?F. OSM E is characterized by *M. lappi* (*M.* cf. *lappi* in the early part), *M. minor* and in its late part the first *Cricetodon*. In OSM E′ the large sized *Megacricetodon* lineage went extinct and in OSM F and ?F the molar size increase in the *Cricetodon* lineage allows a further subdivision.

## Research results

### Sections and lithology

Descriptions are given of the main sedimentological and lithological characteristics of the western Bavarian sections (Fig. 2), including the outcrops containing volcanic ashes.

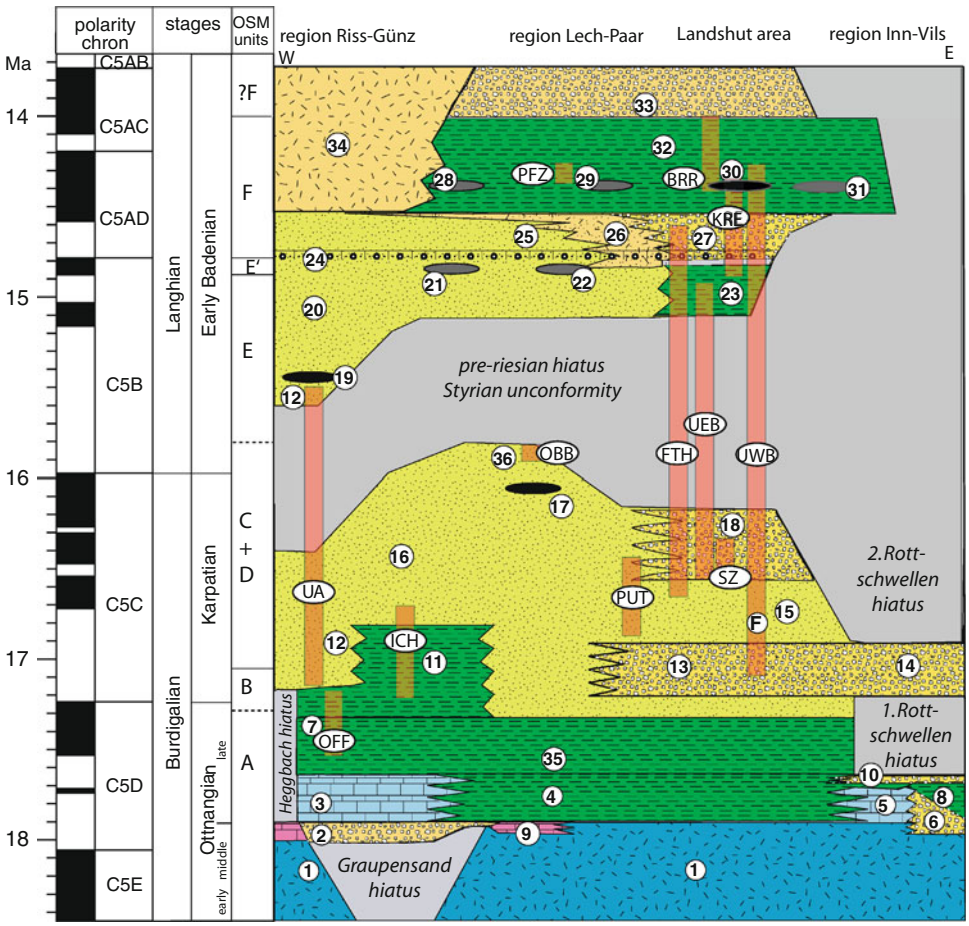


**Fig. 2** Synoptic chart of the proposed chronology for the Lower to Middle Miocene sediments in the Bavarian part of the NAFB: lithostratigraphic units (according to Doppler et al. 2005; UL *Limnische Untere Serie*, UF *Fluviatile Untere Serie*, NV *Nördlicher Vollschotter*) and stratigraphic coverage of studied sections (red bars; including those from the eastern part of the basin, see Abdul Aziz et al. 2008; for the geographic position of sections see Fig. 1). *1* Marine Molasse, *2* Grimmelfingen beds, *3* Kirchberg Formation, *4 Sand–Kalkmergel–Serie* and *untere Bunte Mergel Serie*, *5* Oncophora beds, *6* Ortenburg gravel, *7* UL at Offingen, *8* limnic freshwater beds, *Feinkörnige Deckschichten*, *9 Albstein*, *10* fluvial freshwater beds, *11* UL at Ichenhausen, *12* UF at Untereichen-Altenstadt, *13* NV lower part, *14 Quarzrestschotter*, *15 Süßwasserkalk*, *16* UF at Burtenbach, *17* Zahling-2 glass-tuff, *18* NV early upper part, *19* Krumbad bentonite, *20* UF at Mohrenhausen, *21* Oberschöneberg bentonite, *22* Unterneul bentonite, *23 Zwischenmergel*, *24* Brock-horizon, *25* UF at Ziemetshausen, *26 Geröllsande*, *27* NV late upper part, *28* Thannhausen bentonite, *29* Laimering bentonite, *30* Landshut area bentonites, *31* Lower Bavarian bentonites, *32 Sand-Mergel-Decke*, *33* Lower Laimering Series, *Übergangsschichten*, *34 Steinbalmensande*, *35 obere Bunte Mergel-Serie*, *36* UF at Oberbernbach. *OFF* Offingen section, *ICH* Ichenhausen section, *UA* Untereichen-Altenstadt section, *PUT* Puttenhausen section, *FTH* Furth section, *UWB* Unterwattenbach section, *UEB* Unterempfenbach section, *SZ* Sandelzhausen section, *BRR* Bruckberg section, *PFZ* Pfaffenzell section, *OBB* Oberbernbach section, *KRE* Kreut section. Colors: *light gray* hiatus, *blue* marine sediments, *light blue* brackish sediments, *pink* paleosols, *green* fine-grained freshwater sediments, *light green* sands, *yellow and orange* coarse-grained sediments. *Black ellipses* indicate $^{40}Ar/^{39}Ar$-dated volcanic ashes, *gray ellipses* are non-dated ashes. (Note that the chronology of sediments older than 17.6 Myr is still tentative)

For descriptions of the eastern Bavarian sections we refer to Abdul Aziz et al. (2008).

Puttenhausen (PUT) section is located in the eastern part of the study area (48°36.74′N and 11°46.36′E). As the paleomagnetic results of the first sampling campaign in 2004 were unclear (see Abdul Aziz et al. 2008), we re-sampled and extended the PUT section. The section belongs to the lower part of the NV lithostratigraphic unit and comprises an 18 m thick succession of fine-grained fluvial–alluvial sediments, which show a regular alternation of blue–gray sands and silts and (purple-)red to yellow brown paleosols (Fig. 4). At least six paleosols yielded fossil vertebrate remains (Puttenhausen A to E). The lowermost horizon, PUT A, contains the classic Puttenhausen fossil level of Fahlbusch and Wu (1981) (Table 1).

On the southern edge of the Danube Valley and about 25 km north of Ichenhausen, the blue–gray sediments of the Offingen (OFF) section (Fig. 1, 48°28′25.90″N and 10°21′25.89″E) crop out in a 15 m deep quarry. A study of

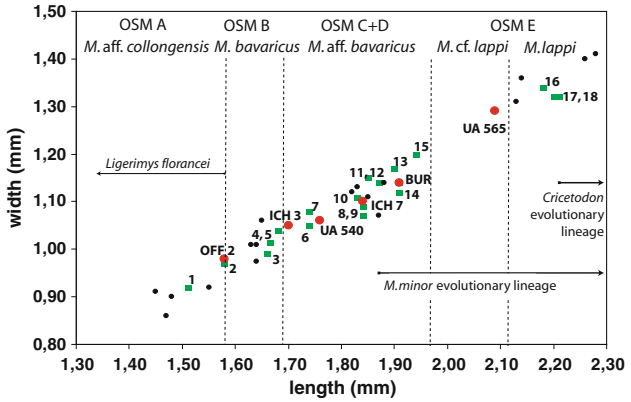


**Fig. 3** Length–width diagram of the first lower molar (mean values) within the large sized *Megacricetodon* evolutionary lineage of 42 Upper Freshwater Molasse localities from Southern Germany and the relative positions of the *M. minor* and *Cricetodon* evolutionary lineages. Large red dots represent the new samples from the western part of the Molasse (*OFF 2* Offingen 2, $n = 3$; *ICH 3, 7* Ichenhausen 3, 7, $n = 6$, $n = 4$; *UA 540, 565* Untereichen-Altenstadt 540 m, 565 m, $n = 6$, $n = 22$) and green squares important localities mentioned in the text (*1* Forsthart, $n = 12$; *2* Günzburg 2, $n = 8$; *3* Langenmoosen, $n = 33$; *4* Bellenberg 1 + 2, $n = 85$; *5* Niederaichbach, $n = 2$; *6* Engelswies/Schellenfeld, $n = 12$; *7* Roßhaupten, $n = 9$; *8* Bubenhausen, $n = 44$; *9* Puttenhausen B, $n = 3$; *10* Puttenhausen classic, $n = 17$; *11* Edelstetten, $n = 13$; *12* Gisseltshausen 1b, $n = 4$; *13* Oggenhof, $n = 3$; *14* Burtenbach 1b + 1c, $n = 48$; *15* Sandelzhausen, $n = 13$; *16* Affalterbach, $n = 15$; *17* Furth 460 m, $n = 1$; *18* Mohrenhausen, $n = 13$; *19* Ebershausen, $n = 7$). The small black dots represent other Bavarian localities. Note the sample gap between OSM C + D and OSM E as a result of the pre-Riesian hiatus

borehole sediments drilled close to the quarry (Doppler 1989, fig. 17) indicates that the base of the sedimentary succession at Offingen lies 35 m above the top of the Kirchberg Formation, a brackish water sequence of fossil-rich marls, sands, and limestones (Reichenbacher 1989). As a result, the OFF section correlates to the older part of the UL (Doppler 1989). In the section, several 10–20 cm thick dark gley paleosols (interpreted as pedogenic Ah-horizons by Maurer and Buchner 2007) are intercalated within the marly, blue–gray, fluvio-limnic fine-grained clastics (crevasse splay deposits of Maurer and Buchner 2007; Fig. 4). They often show a fining-up trend from blue gray sands to silts, muds and finally dark organogenic gley paleosol horizons. These horizons also show small channel like features (max. 2 m wide) of which the base is rich in fossil shells and vertebrate remains (OFF 2: Fig. 4; Table 1). Finally, the studied section also comprises rare calcareous layers, indicative of pedogenesis (pseudogley paleosols, Maurer and Buchner 2007).

The Oberbernbach (OBB) section (48°28.39′N and 11°06.50′E) is located west of Augsburg (Fig. 1). According to the local stratigraphy, this section belongs to the UF unit (Doppler 1989) and comprises an approximately 5 m thick fluvial–alluvial sequence of red to yellow–brown paleosols alternating with, often yellow mottled, gray sands and silts (Fig. 4). The red paleosols are interpreted as mature soils which developed distally from the river channel while the less mature yellowish paleosols are interpreted as poorly drained soils which developed close to the channel (Kraus and Aslan 1993). In addition, the color mottling of the sands and silts suggest that, probably after channel abandonment, these deposits also underwent some pedogenic modification. The upper part of the section comprises a ~1.5 m thick unconsolidated gray–blue sand unit, which is topped by recent soils. The two fossil sites OBB A and OBB B are associated with red paleosols (Fig. 4).

The approximately 45 m long Untereichen-Altenstadt (UA) section (48°10.23′N and 10°06.50′E) also belongs to the UF (Doppler 1989). The UA section is the most western located section and lies south of Ulm. The section can be subdivided into two distinct units: a 30 m thick lower blue–gray marly unit and a 15 m thick upper yellow sandy unit. The lower unit comprises blue–gray marly, fine- to medium grained sands, silts, and muds which alternate with yellow–brown, and sometimes red, mottled paleosols (Fig. 5). The sand and silt beds, which gradually increase in the upper part of the marly unit, are interpreted as crevasse splay, overbank, channel, and floodplain deposits of a low-energy, meandering fluvial system (see Maurer and Buchner 2007; Pretor et al. in press for details). The yellow–brown mottled paleosols are interpreted as poorly drained hydromorphic soils, which presumably developed close to the channels, whereas the red paleosols represent more mature soils which developed in the distal parts of the fluvial-floodplain. The fossil vertebrate remains of site UA 540 m, representing a collapsed animal burrow (see Prieto et al. 2009; Fig. 13), were found in the top part of a red–brown paleosol (Fig. 5). The yellow upper sandy unit conformably overlies the blue–gray marly unit forming a sharp color contrast. The sandy unit is dominated by 15 m thick, poorly consolidated yellowish, medium-grained succession of sands. A variety of channel facies occur such as trough cross-beds, sand bars, sub-aqueous dunes, and overbank sands, which are interpreted as deposits of a low-energy sandy braided river system (see Prieto et al. 2009). The fossil site UA 565 m is situated halfway this sandy unit (Fig. 5).

Northeast of the UA section, the sedimentary succession of Ichenhausen (ICH) section (48°22.49′N and 10°19.07′E) is exposed in a more than 20 m deep quarry. The monotonous marly blue–gray deposits correspond to the UL lithostratigraphic unit (Doppler 1989) and often comprise a fining-up sequence of (very) fine-grained sands, silts, and muds. On top of the muds 10–30 cm thick dark marly layers are discernable often rich in fossil shell, vertebrate, and fish remains (Fig. 5). Fine-grained dispersed organic

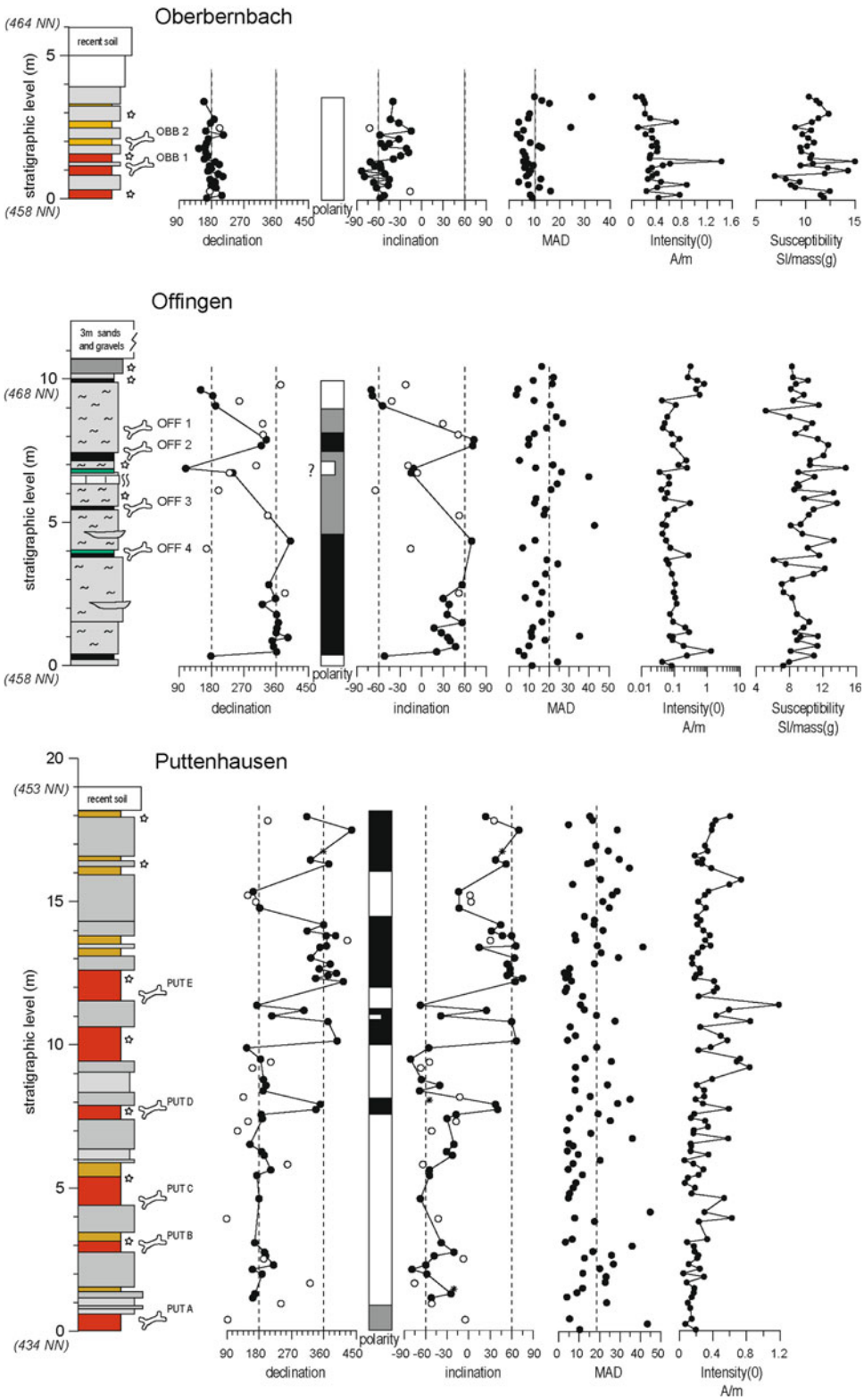


**Fig. 4** Lithological logs and paleomagnetic results of the OBB, OFF and PUT sections. In the lithological logs, gray shades represents gray muds, silts and sands (marls are indicated with ~); the *red* and *orange* coloring represent paleosols; *stars* along the log indicate color mottling with (occasionally) carbonate nodules and *bones* indicate position of small-mammal fossil localities. The *black* (white) dots in the declination and inclination records represent reliable (uncertain) ChRM directions. In the polarity columns, *black* (white) zones indicate normal (reversed) polarity and *gray shaded zones* undefined polarity. *MAD* indicates Mean Angular Deviation

material together with pyrite minerals are often found throughout the blue–gray succession. Occasionally, bioturbation traces can be found. The stratigraphic interval between 13 and 16 m is characterized by millimeter-laminated blue–gray fine-grained sands indicating that deposition took place in a (full) lacustrine environment. At least four dark marls contained small-mammal fossil remains (see Fig. 5; Table 1). The fine-grained UL

**Table 1** Ectothermic vertebrates and small-mammals from the localities Burtenbach (BUR 1b), Ichenhausen (ICH 3 and 7), Offingen (OFF 2 and 4), Puttenhausen (PUT A), and Untereichen-Altenstadt (UA 540 m and 565 m)

| | | | OSM C+D | | | | | | | OSME |
|---|---|---|---|---|---|---|---|---|---|---|
| | | | OFF 4 | OFF 2 | ICH 3 | UA 540m | ICH 7 | PUT cl. | BUR 1b | UA 565m |
| **Rodentia** | Cricetidae | *Megacricetodon bavaricus* | | | aff. | aff. | aff. | aff. | aff. | |
| | | *Megacricetodon lappi* | | | | | | | | aff. |
| | | *Megacricetodon minor* | | | | | | | cf. | aff. |
| | | *Democricetodon gracilis* | | | | | | | | |
| | | *Democricetodon mutilus* | | | | | | | | |
| | | *Eumyarion bifidus* | | | | | | | cf. | |
| | | *Eumyarion* weinfurteri | | | | | | cf. | cf. | |
| | | *Eumyarion medius* | | | | | | | | |
| | | *Neocometes* sp. | | | | | | | | |
| | Anomalomyidae | *Anomalomys minor* | | | | | | | | |
| | Eomyidae | *Keramidomys thaleri* | | | | | | | | |
| | Gliridae | *Microdyromys complicatus* | | | | | | | cf. | cf. |
| | | *Glirulus diremptus* | | | | | | | | |
| | | *Prodryomys satus* | | ? | | | | | | |
| | | *Miodyromys aegercii* | | | | aff. (?) | | aff. | cf. | aff. |
| | | *Miodyromys biradiculus* | | aff. | aff. | | aff. | | | |
| | | *Bransatoglis astaracensis* | | | | | | | | |
| | | *Bransatoglis cadeoti* | | | | | | | | |
| | | *Glirudinus* cf. *undosus* | | | | | | | | |
| | | *Glirudinus* sp. | | | | | | | | |
| | | *Paraglirulus* aff. *werenfelsi* | | | | | | | | |
| | | Gliridae indet. sp. 1 | | | | | | | | |
| | | Gliridae indet. sp. 2 | ? | | | | | | | |
| | Sciuridae | *Spermophilinus besanus* | | | | | | | sp. | |
| | | *Paleosciurus sutteri* | | | | | | | sp. | |
| | | *Heteroxerus* aff. *rubricati* | | | | | sp. | | sp. | |
| | | *Blackia miocaenica* | | | | | | | | |
| | | *Miopetaurista dehmi* | | | | | | | sp. | |
| | Castoridae | *Steneofiber depereti* | | | | | | | cf. | |
| **Lagomorpha** | | *Prolagus oeningensis* | ? | | | | ? | ? | | |
| | | *Prolagus crusafonti* - like form | | | | | | ? | | |
| | | *Amphilagus* sp. | | | | | | ? | | |
| | | *Lagopsis verus* | | | | | | | | |
| | | *Lagopsis* penai | | | | | | cf. | | |
| **Marsupialia** | Didelphidae | *Amphiperatherium frequens* | sp. | | | | | n. ssp. | | |
| **Lipotyphla** | Soricidae | *Dinosorex zapfei* | | | | | | aff. | sp. | cf. |
| | | *Dinosorex*/*Heterosorex* sp. | | | | | | | | |
| | | *Lartetium dehmi* | | | | | | ? | | |
| | | *Limnoecus* n. sp. | | | | | | | | |
| | | Soricidae indet. (several species) | | | | | | | | |
| | Dimylidae | *Plesiodimylus chantrei* | | | | | | | sp. | |
| | Talpidae | Talpidae indet. (or several species) | | | | | | | | |
| | | *Prosacapanus sansaniensis* | | | | | | | sp. | |
| | Erinacidae | *Galerix exilis* | sp. | sp. | sp. | cf. | sp. | aff. | sp. | cf. |
| | | *Lanthanotherium sansaniensis* | | | | | | aff. | | aff. |
| | | *Mioechinus* sp. | | | | | | | | |
| **Chiroptera** | | Chiroptera indet. (several species) | | | | | | | | |
| **Cypriniformes** | Cyprinidae | Cyprinidae indet. | | | | | | | | |
| | | *Palaeocarassius* sp. | | | | | | | | |
| | | *Palaeocarassius mydlovariensis* | | | | | | | | |
| | | *Palaeoleuciscus* sp. A | | | | | | | | |
| | | *Palaeoleuciscus* sp. B | | | | | | | | |
| | | *Barbus* s.l. sp. B | | | | | | | | |
| **Channiformes** | Channidae | *Channa sp.* | | | | | | | | |
| **Perciformes** | Gobiidae | *Gobius sp.* | | | | | | | | |
| **Allocaudata** | Albanerpetontidae | *Albanerpeton inexpectatum* | | | | | | | | |
| **Urodela** | Salamandridae | *Salamandra sansaniensis* | | | | | | | | |
| | | *Chelotriton* sp. | | | | | | | | |
| | | *Triturus (vulgaris)* sp. | | | | | | | | |
| | Proteidae | *Mioproteus caucasicus* | sp. | sp. | | | sp. | | | sp. |
| **Anura** | Discoglossidae | *Latonia gigantea* | sp. | | sp. | sp. | | | | |
| | | *Latonia ragei* | | aff. | | | | | | |
| | Pelobatidae | *Eopelobates* sp. | | | | | | | | |
| | | *Pelobates* sp. | | | | | | | | |
| | Ranidae | *Pelophylax* sp. | | | | | | | | |
| | | *Pelodytes* vel *Bufo* | | | | | | | | |
| | | Anura indet. | | | | | | | | |
| **Crocodylia** | Alligatoridae | *Diplocynodon styriacus* | | | | | | | | |
| **Chelonia** | Trionychidae | *Trionyx (triunguis)* sp. | | | | | | | | |
| | Geoemydidae | *Clemmydopsis turnauensis* | | | | | | | | |
| | Emydidae | *Mauremys* sp. | | | | | | | | |
| | Testudinidae | *Testudo* sp. | | | | | | | | |
| | | *Ergilemys* sp. | | | | | | | | |
| | | Chelonia indet. | | | | | | | | |
| **Iguania** | Chamaeleonidae | *Chamaeleo bavaricus* | | | | | | | | |
| | | *Chamaeleo* sp. | | | | | | | | |
| | Agamidae | Agamidae indet. | | | | | | | | |
| **Scincomorpha** | Lacertidae | *Lacerta* s.l. sp. 1 | | | | | | | | |
| | | *Lacerta* s.l. sp. 2 | | | | | | | | |
| | Scincidae | Scincidae indet. 1 | | | | | | | | |
| | Cordylidae | Cordylidae indet. | | | | | | | | |
| | | Scincomorpha indet. 1 | | | | | | | | |
| | | Scincomorpha indet. 2 | | | | | | | | |
| **Anguimorpha** | Anguidae | *Ophisaurus* sp. | | | | cf. | | | | |
| | | *Pseudopus laurillardi* | | | | | | | | |
| | | *Anguis* sp. | | | | | | | | |
| | | Anguidae indet. | | | | | | | | |
| **Amphisbaenia** | Amphisbaenidae | Amphisbaenidae indet. | | | | | | | | |
| **Serpentes** | | Serpentes indet. | | | | | | | | |
| | Viperidae | Viperidae indet. | | | | | | | | |
| | Natricidae | Natricidae indet. | | | | | | | | |
| | Colubrinae | Colubrinae indet. (small) | | | | | | | | |
| | | Colubrinae indet. (large) | | | | | | | | |

PUT according to Abdul Aziz et al. (2008), UA according to Prieto et al. (2009). BUR, ICH and OFF this paper

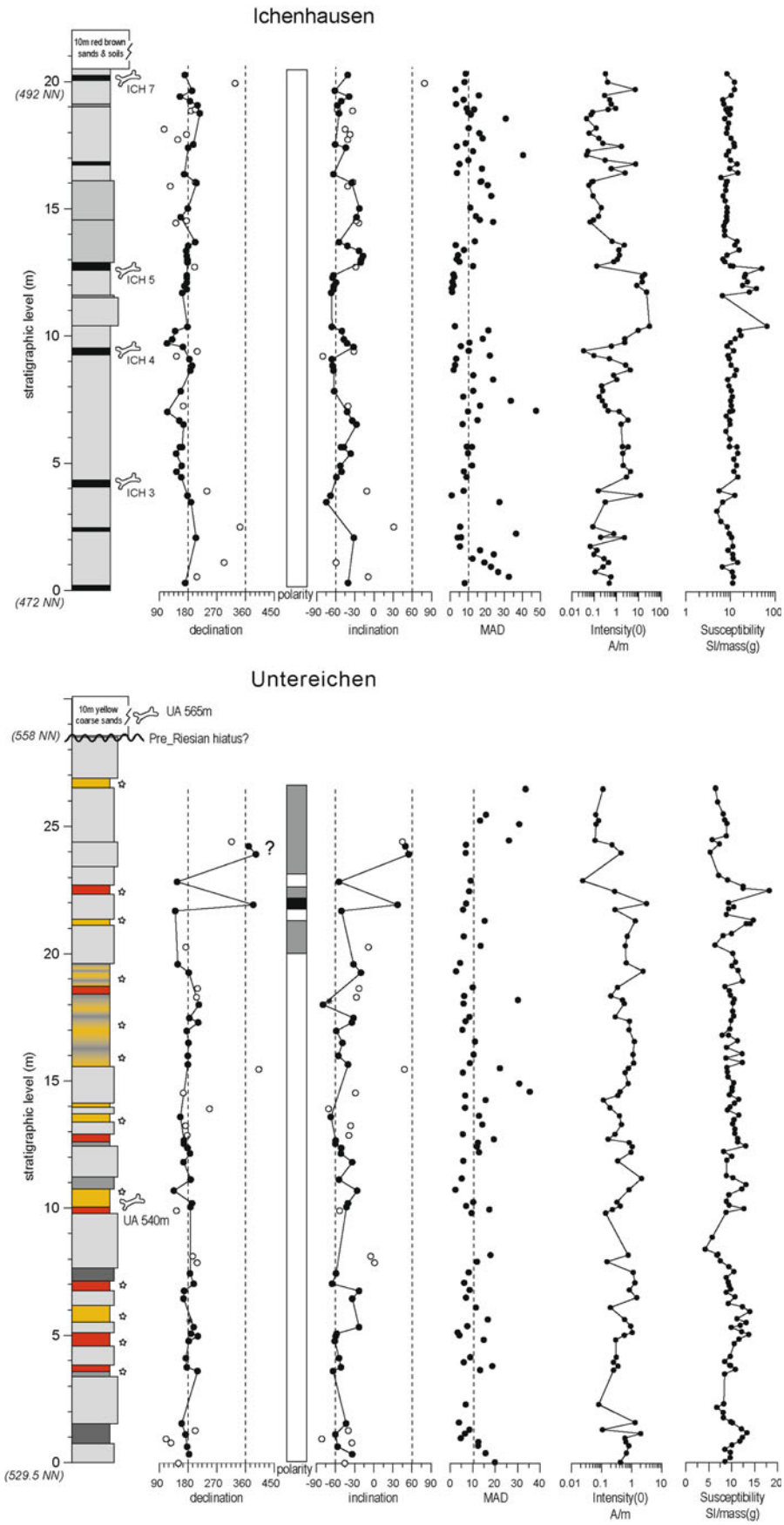


**Fig. 5** Lithological logs and paleomagnetic results of the ICH and UA sections. For details see caption of Fig. 5

sediments are erosive overlaid by yellow sands of the UF lithostratigraphic unit (Doppler personal communication).

*Volcanic ash sites*

Two volcanic ashes are studied from the West-Molasse for $^{40}Ar/^{39}Ar$ dating technique. The first is the glass-tuff of Zahling-2 (Zahling-2 outcrop in Fig. 6) 12 km northeast of Augsburg. This 7 m thick tuff is thought to belong to the "main-bentonite layer" in the Augsburg-Dasing area (Schmid 1994; Ulbig 1994; Heissig 2006). However, re-investigation of the outcrops around Zahling reveals that the tuff belongs to an older stratigraphic unit than the widespread bentonites ("main bentonite", Fig. 6). Approximately 400 m west of Zahling-2, on the top of the gravel pit Zahling 1, a 2 m thick bentonite is recovered in the typical lithostratigraphic position for the Augsburg-Dasing "main-bentonites", that is above a medium-grained carbonate poor gravel which is overlain by sandy and marly sediments. This local succession below the "main bentonite" corresponds to the *Gallenbacher Schotter* and the *Sand–Mergel–Decke* described by Fiest (1989). The base of the Zahling 1 bentonite is at 512 m NN, whereas the base of the Zahling-2 glass-tuff is at 505 m NN (Schmid 1994). Furthermore, below the bentonite, within the *Gallenbacher Schotter*, several large (up to 30 cm in diameter) bentonite clasts have been found by the authors in 2007, which probably represent eroded and bentonitized glass-tuff fragments. Considering the different lithology of both volcanic deposits, the bentonite and the glass-tuff most probably do not belong to the same horizon; rather the glass-tuff is older than the bentonite horizon. Taking into account the $^{40}Ar/^{39}Ar$ dating results (see below) it seems plausible that the volcanic ashes are separated by the pre-Riesian hiatus (see below), which left a significant paleo-relief of about 30 m in this area (Fig. 6).

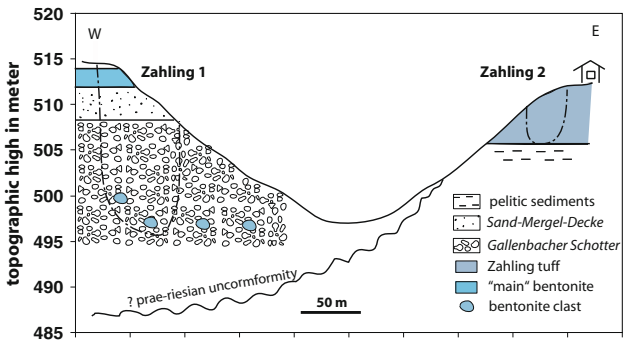


**Fig. 6** Geologic sketch around Zahling indicating the different stratigraphies of the Zahling 1 ("main"), bentonite (gravel pit Zahling) and Zahling-2 tuff (outcrop in the village), and the assumed position of the pre-Riesian unconformity

The second sampled volcanic ash is the 6 m thick bentonite and glass-tuff of Krumbad (Ulbig 1994), which is interbedded within the UF lithostratigraphic unit (Doppler 1989). Also here it was assumed that these deposits correlate to the "main-bentonite layer" of the Augsburg and Landshut areas (Scheuenpflug 1980; Ulbig 1994). A detailed investigation of the position of the Brock-horizon relative to the bentonite challenges this assumption. The base of the Krumbad bentonite is at 540 m NN while the nearest Brock-horizon at Hohenraunau (3.3 km SSW of Krumbad) is at 537 m NN. Considering the dip of the basin sediments to the south–southeast (according to Doppler 1989, p. 91 6–9 m/km) it follows that the Krumbad bentonite should be situated below the Brock-horizon. This interpretation is further confirmed by our new $^{40}Ar/^{39}Ar$ dating results (see below).

In addition to these two ashes, we also analyzed the rhyolitic-dacitic *Basisbentonit* of the Hegau volcanic area from the locality Heilsberg. The sample is derived from a greenish white glass-tuff on the eastern slope of the Heilsberg about 1.5 km north of Gottmadingen (Hofmann 1956; Harr 1976). This ash layer is embedded into Upper Freshwater Molasse sediments (probably *Oberer Haldenhofmergel*; Hofmann 1956, p. 114, Doppler et al. 2005), which are overlain by pisolitic pyroxenic tuffs (*Deckentuffe*). The ashes correspond to the nearby located glass-tuff of Riedheim (3.5 km northwest of Heilsberg outcrop, southern slope of the Hohenstoffeln; Engelhardt 1956; Harr 1976) and to the glass-tuff of Bischoffszell (45 km southeast of Heilsberg, Hofmann 1951, fig. 1). K/Ar dating of sanidine crystals from Bischofszell gives an age of 14.6 ± 0.7 Ma (Gentner et al. 1963), leading Lippolt et al. (1963, p. 529) to the assumption of contemporaneous deposition with the main bentonites of lower Bavaria ($^{40}Ar/^{39}Ar$ of glasses 14.55 ± 0,19 Ma, Abdul Aziz et al. 2008). Bolliger (1992, p. 199) correlates the Bischofszell ashes to the Leimbach bentonites, which are dated by single zircon U/Pb technique to 14.2 Ma (Gubler et al. 1992).

## Biostratigraphy

For the biostratigraphy of the re-sampled Puttenhausen section we refer to Abdul Aziz et al. (2008).

Offingen (OFF) section

The Offingen locality yields the biostratigraphic oldest small-mammal assemblage of all studied sections. The *Megacricetodon* population at level OFF 2 is more primitive than *M. bavaricus* from Langenmoosen (OSM B), more evolved than *M.* aff. *collongensis* from Forsthart (Fahlbusch and Ziegler 1986; OSM A), and corresponds in

size to *M.* cf. *bavaricus* from Günzburg 2 (Reichenbacher et al. 1998; OSM A). The Forsthart and Günzburg 2 localities yield the biostratigraphically important eomyid *Ligerimys florancei*, which is absent in OFF 2 (Table 1). The absence could be either attributed to the small sample size, unfavorable ecologic conditions, or indicate a slightly younger biostratigraphic age. The latter seems most possible, because after Reichenbacher et al. (1998) the Günzburg 2 level is about 15 m above the top of the Kirchberg Formation (Brackish Water Molasse), whereas the base of the Offingen section lies about 20 m higher (see above). The OFF 2 level is placed at the OSM A/B transition (Figs. 2, 3).

### Oberbernbach (OBB) section

The samples OBB A and B were taken as test samples during the paleomagnetic fieldwork 2006. In OBB A, a small *Megacricetodon* species probably belonging to *M. minor* was found, whereas in OBB B a single molar of *Megacricetodon* aff. *bavaricus* was detected (Table 1). The association of two *Megacricetodon* species is characteristic for faunas from the late OSM C + D (Gisseltshausen 1b and younger, Figs. 2, 3) and OSM E, however, the lack of additional material does not allow a more precise biostratigraphic characterization than late OSM C + D.

### Untereichen-Altenstadt (UA) section

The biostratigraphy of the UA section is in detail discussed in Prieto et al. (2009) and is only summarized here. The level UA 540 m corresponds to the early part of OSM C + D (Fig. 3). It is older than the classic level of Puttenhausen (Abdul Aziz et al. 2008) and younger than Langenmoosen (Fahlbusch 1964), Bellenberg 1, 2 (Boon 1991), Niederaichbach (Schötz 1993), and Ichenhausen 3 (this article). The biostratigraphy corresponds best to the Swiss locality Hüllistein (Bolliger 1992), the German locality Rosshaupten (Fahlbusch 1964), and approximately to Engelswies/Schellenfeld (Ziegler 1995), the latter being only somewhat older.

Sample UA 565 m corresponds to the early part of OSM E (Figs. 2, 3). It is older than Mohrenhausen, Ebershausen (Boon 1991), Furth 460 m (Abdul Aziz et al. 2008) and the localities Grund and Mühlbach from the marine Early Badenian Grund and Gaindorf Formations of the Central Paratethys (upper part of Lower Lagenid zone, late M5b-M6, ~15.1 Ma; Rögl et al. 2002; Rögl and Spezzaferri 2003; Ćorić et al. 2004). UA 565 m is younger than the late Karpatian faunas from the late OSM C + D (e.g., Sandelzhausen, Oggenhof, and Affalterbach; Abdul Aziz et al. 2008) and can be correlated to the early Badenian. It represents the oldest biostratigraphically dated locality of the Middle Series.

### Ichenhausen (ICH) section

We found four superposed fossil bearing levels in the section (Fig. 5). Two of them (ICH 3 and ICH 7) have a rich small-mammal record (Table 1; Fig. 7). The size of the *Megacricetodon* aff. *bavaricus* population of ICH 3 is in between the populations of Engelswies/Schellenfeld, Langenmoosen and Bellenberg 1 + 2 and smaller than UA 540 m. This suggests a biostratigraphic position near the base of OSM C + D (Fig. 3).

The level of ICH 7 at the top of the section yields a relatively large sized *Megacricetodon* aff. *bavaricus.* It is of the same size like PUT cl., PUT B (Abdul Aziz et al. 2008), Jettingen (Fahlbusch 1964), Bubenhausen and Edelstetten (Boon 1991) and somewhat smaller than Gisseltshausen 1b, Sandelzhausen (Abdul Aziz et al. 2008), and Burtenbach 1b + 1c (see below). A second, smaller sized *Megacricetodon* species is missing. The data indicate a biostratigraphic position in the latest part of the early OSM C + D (Fig. 3) and a significant younger age than ICH 3.

### Burtenbach locality

The small-mammals of the Burtenbach locality (Table 1) were studied because of their regional importance. The sand pit Burtenbach is situated 10 km SE of ICH section. The sediments belong to the UF sedimentary unit and are correlative to the UF sand at the top of the ICH section. The exceptional rich fauna yield a *Megacricetodon* aff. *bavaricus* population, which is evolutionary nearly identical to Sandelzhausen and somewhat younger than ICH 7 just below the UF sands in the ICH section. In addition, a second, small sized *Megacricetodon* species is present

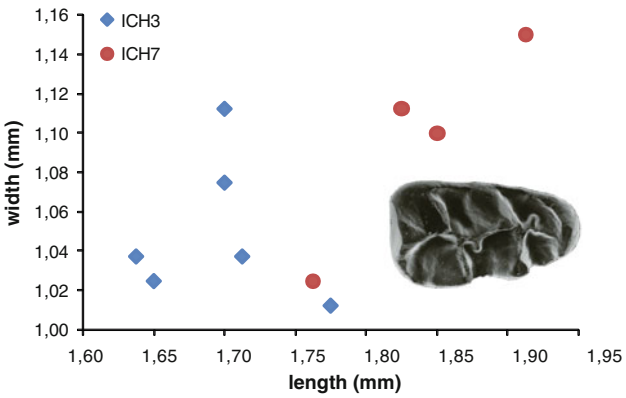


**Fig. 7** Scatter diagram of the first lower molar of *Megacricetodon* aff. *bavaricus* from the Ichenhausen section

(*M*. cf. *minor*, Table 1), which confirms the correlation with Sandelzhausen (Fig. 3) and places the locality in the late OSM C + D.

Another nearby locality from the UF is Jettingen (8.8 km E of Ichenhausen). The *M*. aff. *bavaricus* population, described by Fahlbusch (1964), is of the same size like those from ICH 7 (latest part of early OSM C + D). These results suggest that the UF lithostratigraphic unit in the region between Ichenhausen and Burtenbach (along the Mindel and Günz valleys) belong to the transition from the early to late part of OSM C + D.

## $^{40}$Ar/$^{39}$Ar dating

### Samples and methods

In the present study, volcanic glasses from bentonite horizons at Zahling-2, Krumbad, and Heilsberg/Hegau (Fig. 1) have been dated using the $^{40}$Ar/$^{39}$Ar technique. The current samples previously have been sampled and described by Ulbig (1994). All analyzed glass fragments are smaller than 250 μm diameter and were separated from the bentonitic clay "matrix" by elutriating and sieving (Ulbig, 1994). Subsequent ultrasonic treatment in distilled water was used to separate the glass shards from clay particles. Under a binocular zoom microscope, the bulk of the glass fragments appear milky-white showing different degrees of translucence, probably reflecting variable degrees of hydration. The major element composition of the glass fragments was determined by electron probe micro-analysis (EPMA). At each of the three sampled localities, unaltered fragments with a colorless, clear, and translucent appearance are highly subordinate and are here interpreted as being not hydrated. About 30–40 mg of such fresh glass shards of each sample were hand-picked under a binocular zoom microscope for $^{40}$Ar/$^{39}$Ar dating. The samples were wrapped in aluminum foil and loaded in 6 mm ID quartz vials. Together with the Fish Canyon Tuff (FCT) sanidine (assumed age: 28.02 Ma, Renne et al. 1998) and Drachenfels DRA (assumed age: 25.26 Ma modified from Wijbrans et al. 1995 for consistency with Renne et al. 1998; following the recommended values for FCT of Kuiper et al. 2008, of 28.201 ± 0.046 Ma, the reported ages would come out ca 0.65% older) monitor standards, the samples were irradiated for 1 h with fast neutrons in the Cd-lined RODEO facility of the EU/Petten HFR Reactor (the Netherlands). Argon isotope analysis was carried out at the Department of Isotope Geochemistry, VU University Amsterdam (the Netherlands), using a MAP 215-50 noble gas mass spectrometer. For all but one sample we applied a single (as opposed to incremental) fusion approach. For each sample, five replicates were fused, while incremental heating included ten temperature steps. As to Zahling-2, two different size-fractions of 150–200 and 200–250 μm, respectively, were analyzed by total fusion and an additional mixed size fraction by incremental heating. For Heilsberg, both a glass and an alkali feldspar sample were analyzed by total fusion. Further details regarding sample preparation and analytical conditions are given in Abdul Aziz et al. (2008).

### Results

Table 2 lists the mean major element composition of the investigated glasses from Krumbad, Zahling 2, and Heilsberg, as determined by EPMA. The Table also includes, for comparison, data for the 14.6 Ma old glasses from the Hachelstuhl bentonite, eastern Bavarian Molasse, previously published in Abdul Aziz et al. (2008). The Table indicates that the total of major element concentrations is lower by a few percent. This effect is probably due to the highly vesiculated structure of the volcanic glasses caused by exsolution of magmatic gases at the sub-μm to μm-scale mirroring the plinian eruption style of the magmas. In addition, partial loss of Na during hydrous alteration or beam evaporation effects during EPMA analysis may have lowered the total sum. The EPMA data indicate an overall rhyolitic composition with respect to the glassy matrix of the magmas. Despite an overall similarity in chemical composition, the samples form two distinct groups that assumingly mirror different degrees of differentiation of at least two different parent magmas. This effect is shown in Fig. 10 which plots the oxides of (Fe + Ti) versus (Na + K + Ca + Al). The two groups are obviously fractionated from each other during crystallization of Fe–Ti-oxides and plagioclase/mica, respectively, in magma chambers. The figure suggests that the Krumbad and Hachelstuhl glasses were derived from chemically less evolved parent magmas when compared to the Zahling and Heilsberg samples. One would, therefore, infer a common eruption center and similar ages for each compositional group. Surprisingly and as shown below, the latter is not the case. Moreover, all glasses have, within error, indistiguishable initial $^{143}$Nd/$^{144}$Nd isotope ratios, ranging between 0.512425 and 0.512430 (Rocholl, unpubl. data). Obviously, no correlation exists between age and chemical or isotopic composition of the glasses. This excludes the feasibility of defining distinct tuffacious stratigraphic marker horizons in the northern alpine molasse on the basis of their geochemistry alone, and emphasizes the necessity of age determination in any single case.

$^{40}$Ar/$^{39}$Ar plateau ages and K/Ca ratios deduced from $^{39}$Ar/$^{37}$Ar ratios of each analytical run are listed in Table 4 (see appendix). Figure 16 (see appendix) shows the

respective weighted mean plateau ages. The black double errors indicate the fractions used for calculating the weighted plateau ages. The diagrams underline the generally high degree of data consistency for a given sample. The exception is the Heilsberg glass that is clearly disturbed by excess argon.

Table 3 summarizes the deduced plateau and isochron ages, with the weighted plateau ages referring to the weighted means over all the accepted data. Three data considered as outliers are indicated in Table 4 and have been excluded from the age calculations. The data for the Hachelstuhl and Ries samples, which were also analyzed in the course of this study, have already been published in Abdul Aziz et al. (2008). For the Ries suevite glass, which served both as an external (i.e., stratigraphic) and internal (i.e., analytical) reference and control of our data, we obtained a weighted plateau age of 14.89 ± 0.10 Ma, which is identical to the normal (14.88 ± 0.11 Ma) and inverse isochron ages (14.84 ± 0.11 Ma). Based on the consistency of plateau and isochron ages, we suggested an age of 14.88 ± 0.11 Ma for the Ries impact event (Abdul Aziz et al. 2008). This age is identical to the mean of 51 published K–Ar, $^{40}Ar/^{39}Ar$, and fission track ages (14.87 ± 0.36 Ma) compiled by Storzer et al. (1995), but notably older than a 14.3 Ma age suggested by Buchner et al. (2003).

In all cases, plateau, isochron, and inverse isochron ages of individual samples are identical within error (Table 3). The exception is the Heilsberg glass for which both isochron ages yielded abnormally large errors. As discussed below, the disturbance is probably due to incorporation of tiny amounts of excess argon in the glass, similar as previously observed for a Hachelstuhl sample (Abdul Aziz et al. 2008). We therefore accept the feldspar data as representative for the Heilsberg sample.

## Discussion and accuracy of the age data

The consistency between obtained isochron ages is by far better than between plateau ages. This is most obvious in case of the three Zahling-2 samples with maximum differences in age of 0.40 Ma and 0.06 Ma for plateau and isochron ages, respectively. Because of the better consistency and the excess argon problem, we prefer the isochron ages over the plateau ages and apply them to our stratigraphic interpretation.

The striking within-sample homogeneity is contrasted by significant differences in age between samples from different localities, ranging up to 1.6 Ma. The data may be classified into three distinct age groups. The oldest one is represented by Zahling-2 with ages of 16.1 ± 0.2 Ma. Hachelstuhl and Heilsberg form the youngest group with ages of 14.5 ± 0.2 Ma. This age compares well with published fission track data of Main Bentonite glasses from Mainburg and Unter-Haarland/Malgersdorf, yielding ages of 14.6 ± 0.8 Ma and 14.4 ± 0.8 Ma, respectively (Storzer and Gentner 1970) and the K/Ar dating of sanidine crystals from the Bischofszell glass-tuff giving an age of 14.6 ± 0.7 Ma (Gentner et al. 1963). An intermediate age group of 15.6 ± 0.4 Ma comprises the Krumbad glasses.

The excellent reproducibility of data obtained for different aliquots of each single sample, different sub-samples or size-fractions (Zahling-2), different analytical approaches (step vs. total fusion, Zahling-2), or different phases analyzed (glass vs. alkali feldspar, Heilsberg), as well as the overall agreement of plateau and isochron ages in most cases strongly suggest that the obtained ages truly refer to the tuffs' eruption and deposition. Nevertheless, our results appear to be in conflict with Fig. 10 which suggests similar ages for Krumbad and Hachelstuhl glasses on the one hand, and Zahling-2 and Heilsberg glasses on the other, which is not the case. There are additional observations that call for critical evaluation of the $^{40}Ar/^{39}Ar$ ages. The fact that the bentonite layers from which the glasses derived had formed by low-temperature alteration of once fresh vitrious tuff, i.e. the glasses themselves, implies that the analyzed glass fragments are residues of this alteration process. K may fractionate from Ar as of function of the degree of hydration and/or alteration, and this process will ultimately affect the calculated ages in such a way that depletion of K relative to Ar will increase the derived age. Also, the later such fractionation occurred with respect to tuff deposition, the stronger the effect on the age calculation will be. Optical and EPMA investigation suggests that there is a spectrum from apparently completely fresh to hydrated to devitrified and altered glass shards. In line with this observation are the results of a stable isotope investigation by Gilg (2005) using this study's samples. The above author suggests that bulk samples, i.e., mixtures of altered/hydrated glasses and their alteration products, had completely exchanged their oxygen with Pleistocene ground waters, a process seriously challenging robust age determination. Although great care has been taken in selecting only completely fresh looking glasses for $^{40}Ar/^{39}Ar$ dating, it cannot be ruled out with absolute certainty that some of the analyzed glass shards have experienced some optically "invisible" K–Ar fractionation that disturbed the age. Fortunately, the possible significance and extent of such alteration-induced K–Ar fractionation can directly be derived from the sample's argon isotope spectrum.

Alteration and possibly also hydration may ultimately fractionate mobile elements such as K from immobile or less mobile elements such as Ca. From neutron-induced $^{39}Ar$ and $^{36}Ar$, produced from K and Ca during irradiation in the reactor, the abundance of K and Ca in the irradiated

sample can be calculated. K/Ca ratios of all total fusion runs, derived from $^{39}Ar/^{37}Ar$ (Table 4) are plotted in Fig. 11 against the plateau ages. The diagram reveals various important correlation effects. First, the oldest ages are obtained for the sample with the highest K/Ca (Zahling 2). This is opposite to what would be expected from hydrated or altered samples having preferentially lost the highly mobile K relative to less mobile elements including Ca. Second, there is no correlation between K/Ca and plateau ages for glasses from different localities. It appears, therefore, impossible to produce the observed range in ages from a single tuff layer by simple alteration. This implies that the measured age differences between tuff layers are real and not the product of secondary processes related to bentonitization. Third, no correlation between K/Ca and age exists for aliquots of single samples, demonstrating both sample homogeneity and analytical reproducibility. There is one notable exception, the Heilsberg glass. Here, a decrease in K/Ca systematically parallels a dramatic increase in age by more than 1.6 Ma, ranging from the youngest to nearly the oldest age of all analyzed samples. Such a trend does not exist in the co-analyzed alkali feldspar fraction. The feldspars are therefore considered as recording the true Heilsberg age, indicating that the two splits with the highest and lowest ages are the main "troublemakers" in the glass fraction. In fact, the 15.7 Ma split (Hb-2a-05; Table 4) has not only the lowest $^{39}Ar/^{37}Ar$ or "K/Ca" (Fig. 11) but also the lowest $^{39}Ar/^{36}Ar$ or "K/Ar" ratio (not shown), and this is compatible with preferential loss of K relative to Ar by glass hydration/alteration. Such a scenario can, however, not explain the very young age of about 14.1 Ma obtained for the high-K/Ca split Hb-2a-01 (Table 4). We, therefore, believe that alteration and hydration alone cannot explain the age systematics of the Heilsberg glasses. Instead, we suggest the presence of tiny amounts excess argon as a more plausible explanation of the observed age disturbance. The argument is based on Fig. 12 in which the $^{36}Ar/^{37}Ar$ or "Ar/Ca" ratios are plotted versus the plateau ages. The diagram shows low and uniform Ar/Ca ratios for all analyzed samples, except for the Heilsberg glasses with argon contents enriched by a factor of 3–9 and systematically decreasing with age, thus demonstrating the influence of excess argon on the obtained ages.

## Summary

Our geochemical and $^{40}Ar/^{39}Ar$ data suggest the following scenario. Highly evolved silicic magmas from a single volcano or volcanic center, characterized by a uniform Nd isotopic composition, erupted repetitively over the course of at least 1.6 Myrs (Figs. 8, 9). The rhyolitic melts tapped

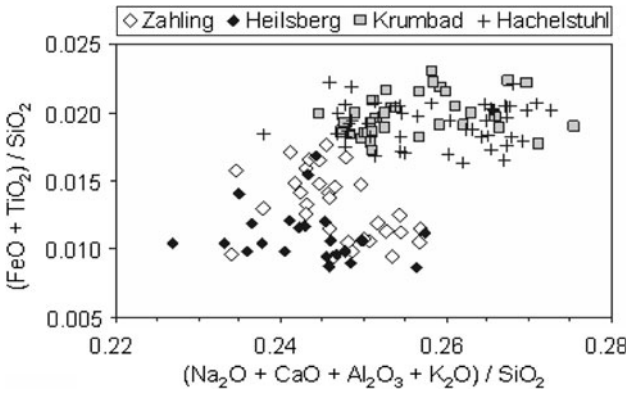


**Fig. 8** (FeO + TiO2)/SiO2 versus (Na2O + CaO + Al2O3 + K2O)/SiO2 ratios in rhyolitic glasses from Miocene bentonite horizons in the Bavarian molasse (Zahling-2, Krumbad, Hachelstuhl) and Hegau, SW-Germany (Heilsberg). Note the grouping into two compositional groups which mirror the contrasting degrees of crystal fractionation (Fe–Ti-oxides, feldspar, mica) in the respective parent magmas

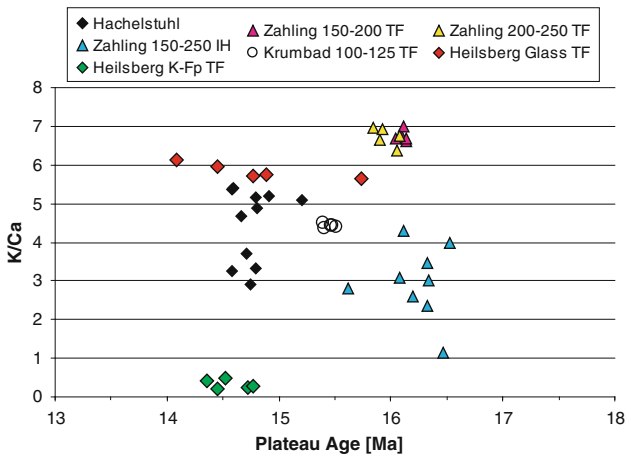


**Fig. 9** K/Ca ratios, derived from $^{39}Ar/^{37}Ar$, in $^{39}Ar/^{40}Ar$-dated rhyolitic tuffs from South Germany. Except for Heilsberg glass, no relationship exists between K/Ca and calculated age

different levels of a stratified magma chamber with different degrees of differentiation. The eruptions were of plinian type and produced wind-driven glassy ashes that settled and accumulated in water-filled depressions in the northern alpine area (Rocholl et al. 2008). Although subsequent alteration to bentonite by interaction with surface and/or ground water affected most of the ash particles, a few remained intact, mostly from the central parts of the deposits, and provided robust $^{40}Ar/^{39}Ar$ ages. Three phases of eruptive activity were identified at 16.1 ± 0.2 Ma (Zahling 2), 15.6 ± 0.4 Ma (Krumbad), and 14.5 ± 0.2 Ma (Heilsberg), the latter eruption phase has been previously identified at Hachelstuhl (Abdul Aziz et al. 2008), Bischoffszell (Gentner et al. 1963), and at Mainburg and Malgersdorf (Storzer and Gentner 1970).

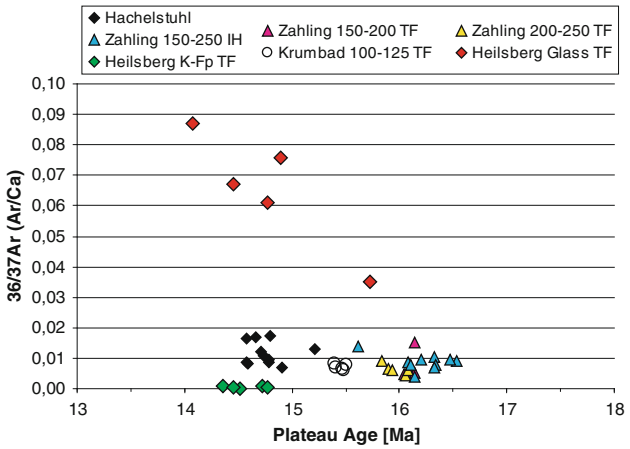


**Fig. 10** $^{36}Ar/^{37}Ar$ ratios mimicking Ar/Ca ratios in rhyolitic tuffs from South Germany. Note the relatively high amount of excess argon in the Heilsberg glasses and the systematic relationship to calculated plateau ages

## Magnetostratigraphy

### Samples and methods

The western Molasse sections were sampled at regular intervals varying between 10 and 25 cm (average 18 cm). Sandy lithologies were mostly avoided because they often produced useless paleomagnetic analysis results (see Abdul Aziz et al. 2008). All the samples were drilled using an electric drilling machine powered by a generator and water as coolant. The initial magnetic susceptibility of the samples was measured on a Kappa bridge KLY-2. The characteristic remanent magnetization (ChRM) was determined by thermal (TH) demagnetization, using incremental heating steps of 20 and 30°C, carried out in a laboratory-built shielded furnace. In order to monitor changes in the mineralogical composition, the bulk magnetic susceptibility was measured after each thermal step on a Minikappa KLF-3 (Geofyzika Brno). The natural remanent magnetization (NRM) was measured on a vertically oriented 2G Enterprises DC SQUID cryogenic magnetometer (noise level $10^{-7}$ A/m) in a magnetically shielded room at the Niederlippach paleomagnetic laboratory of Ludwig-Maximilians-University Munich, Germany. Demagnetization results are plotted on orthogonal vector diagrams (Zijderveld 1967) and ChRM directions are calculated using principal component analysis (PCA, Kirschvink 1980).

### Results

Abdul Aziz et al. 2008 indicated a discrepancy between the ChRM directions from the alternating field (AF) and the TH demagnetization method for the PUT section. Hence, a new sampling campaign was organized, and 102 samples were drilled from a parallel section. The initial NRM intensity of 97 analyzed samples is between 0.048 and 1.2 mA/m (average 0.306 mA/m) (Fig. 4). The lithological variety causes a complex NRM behavior resulting in Zijderveld diagrams of variable quality. About 50% of the diagrams were of good quality enabling a reliable interpretation of the ChRM while at least 33% were of such poor quality that it was impossible to determine their polarity. The good quality diagrams show that a viscous component is removed at 100°C and a second, normal-directed component between 210 and 270°C (Fig. 11a). This normal component possibly represents the present-day field overprint. Depending on lithology, a third component, which is interpreted as the ChRM, is removed between 450 and 480°C (mostly blue gray silts and sands), between 540 and 570°C (sediments with some reddish mottles), and between 600 and 700°C (mostly red paleosols). Although the TH produced better results than the AF demagnetization method, we conclude that the complex NRM behavior observed for the PUT section is likely caused by overlapping components which hampers isolation of the ChRM.

The 79 paleomagnetic analyzed samples from the UA section are all from the blue–gray marly unit, which comprises different fluvial sedimentary environments, consequently, resulting in a variety of magnetic properties. Magnetic susceptibility values for the UA samples are between 4.2 and 18.2 SI/g (average 9.9 SI/g) and initial NRM intensity ranges from 0.023 to 3.15 mA/m (average 0.644 mA/m) (Fig. 5). The Zijderveld diagrams (Fig. 11b) show that a viscous component is removed at 100°C. More than 40% of the samples show a normal overprint (direction 008/65), which is removed in the temperature range of 100–330°C. Depending on sediment type, the yellow and red mottled gray muds and silts comprise a third component which is removed between 670 and 700°C. Other samples, typically consisting of sands and green–gray muds and silts, are demagnetized in the temperature range 390–480°C or around 570°C. We interpret the third component as the ChRM.

The top part of the section, approximately 7 m below the hiatus marking the change to the upper yellow sandy unit, shows a different demagnetization behavior. Most of the (sandy) samples are demagnetized between 270 and 390°C, showing a normal or undeterminable direction (Fig. 5). Since the normal overprint throughout the section is removed around ~330°C, we consider the directions in the upper part unreliable.

In the OBB section, 31 samples were drilled and thermally demagnetized. Susceptibility ranges between 6.87 and 15 SI/g (average 10.6), and initial NRM values range between 0.07 and 1.43 (average 0.4 mA/m) (Fig. 4). Thermal demagnetization of the samples indicates that a

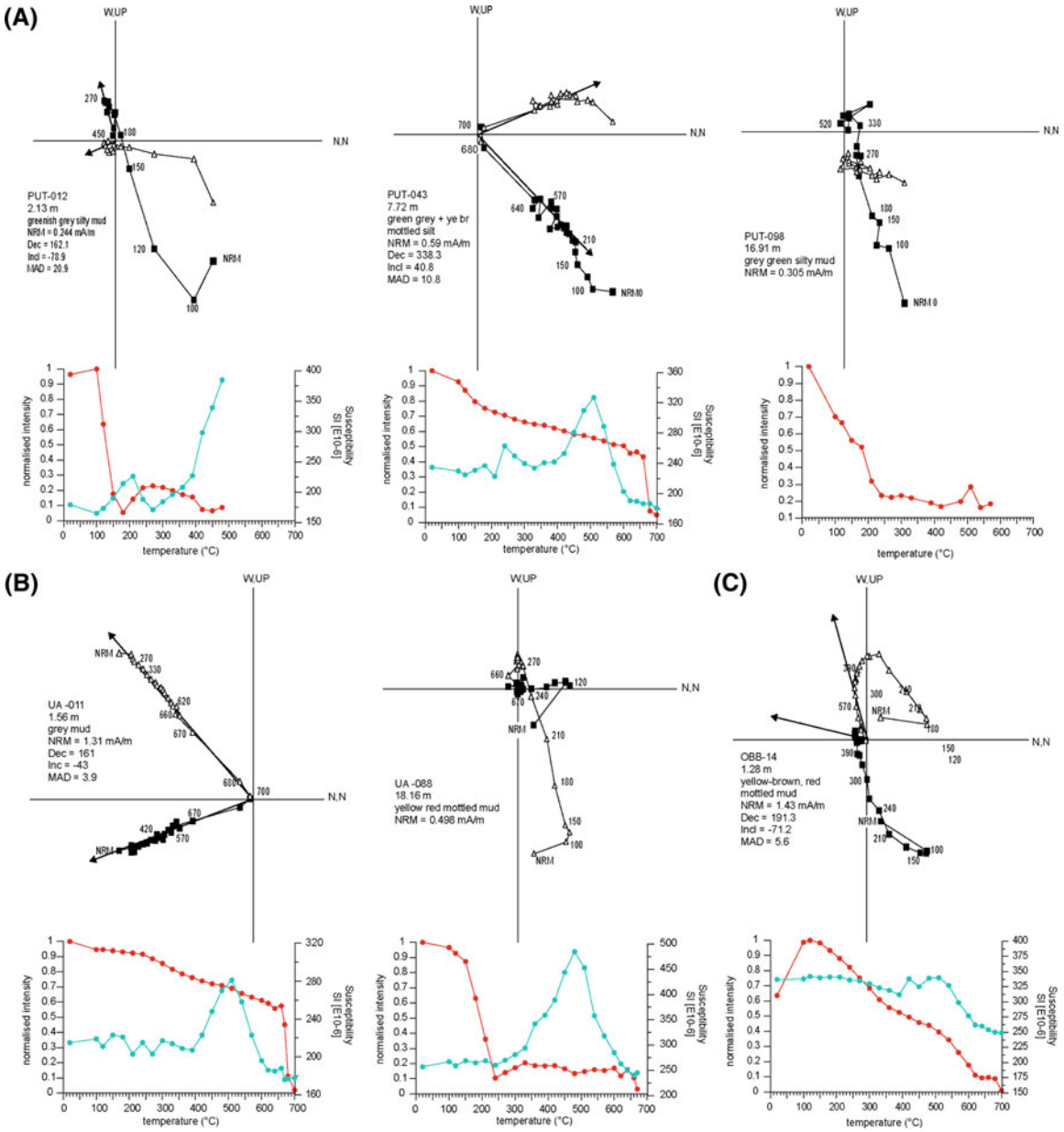


**Fig. 11** Thermal demagnetization diagrams of selected samples from sections in the Western Bavarian Molasse. In the Zijderveld diagrams, *black squares* (white triangles) denote the projection on the vertical (horizontal) scale. Values along demagnetization trajectories indicate temperature steps in °C. Each sample is represented with a susceptibility (*green*) and normalized intensity decay (*red*) curve versus temperature. See text for details

random-oriented viscous component is removed at 100°C. In some samples, a second component is removed between 120 and 150°C suggesting the presence of goethite. Most samples show a third normal component which is removed between temperatures of 180 and 270/300°C (Fig. 11c). The direction of this component (008/62) closely corresponds to the present-day field (1.5/63). Finally, a fourth component is removed between 510 and 680/700°C. The latter two temperatures suggest the presence of (fine-grained) hematite. We interpret this fourth component as the ChRM.

From the 103 drilled samples in the ICH section, 88 were thermally demagnetized. Except for an interval with high initial susceptibility values between stratigraphic levels 10 and 14 m (Fig. 5), the magnetic susceptibility is constant throughout the section (range 5–66, average 11.7 SI/g). NRM values range between 0.05 and 54 mA/m (average 3.01 mA/m). The TH demagnetization diagrams are of good quality with the NRM decaying toward the origin (Fig. 11d). A small viscous component is removed at 100°C and, occasionally, a normal directed overprint is removed around 270°C. Subsequently, two types of

**Fig. 11** continued

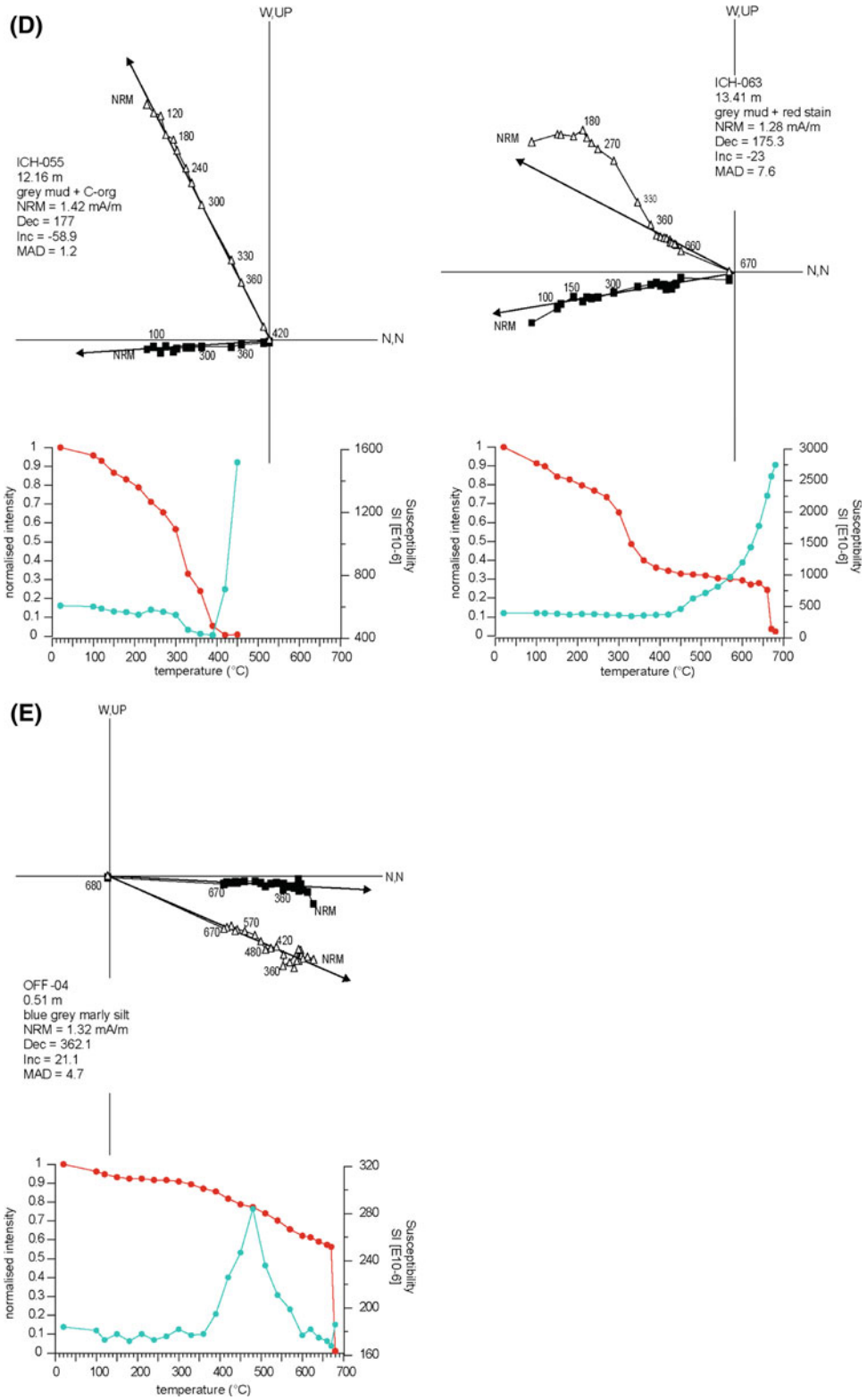


demagnetization behavior can be distinguished: (1) the majority of the samples are completely demagnetized around 420°C, and the associated component is interpreted as the ChRM (average direction 180/53; Fig. 11d) (2) several samples consist of two components, namely a low (LT) and a high temperature (HT) component, which are removed between 330 and 390°C and around 570 or 670°C, respectively (Fig. 11d). Both LT and TH components

decay toward the origin, however, the HT component shows a more gradual decay, sometimes forming a cluster, followed by an abrupt decay at high temperatures. The average direction of the HT component differs only slightly from the LT component (159/42 vs. 169/50) preventing an ambiguous determination of the ChRM. Considering the uniformity of the depositional environment and that the majority of the samples are demagnetized around 420°C, we interpret the LT component as the ChRM.

The initial susceptibility and NRM values are low for the 55 analyzed samples from the OFF section, with values varying from 5 to 15 SI/g and from 0.04 to 1.35 mA/m, respectively (Fig. 4). Thermal demagnetization reveals that a viscous component is removed at 100°C while a second normal directed component is removed between 270 and 300°C. Most samples comprise a third component, which is completely demagnetized at 420°C, or at lower temperatures. Only a few samples are demagnetized around 600°C (Fig. 11e). We interpret this third component as the ChRM.

The susceptibility, magnetic intensity, and ChRM directions for each section are plotted in stratigraphic order and the polarity is interpreted using the mean angular deviation (MAD) of 15° as cut-off (Figs. 4, 5).

### *Magnetic susceptibility*

The magnetic susceptibility, measured after each thermal demagnetization step, for the majority of the samples from all the sections reveals a remarkable uniform behavior (Fig. 12). A slight but distinct increase in magnetic susceptibility is observed between 330°C/360°C and 390°C/420°C. Between 470 and 510°C, the susceptibility decreases again to values often lower and sometimes higher than initial (i.e., prior to 360°C). This increase and subsequent decrease do not seem to affect the magnetization intensity or direction. Conversely, samples with a progressive increase in susceptibility at temperatures >420°C do show changes in magnetization intensity and direction. Since most of these samples are associated with sediments comprising pyrite minerals, the progressive intensity increase after 420°C is likely related to the oxidation of the iron sulfides.

Only a few samples, mostly from PUT section, show stable magnetic susceptibilities up to 520–570°C but when demagnetized at higher temperatures, a slight decrease in susceptibility occurs (e.g., PUT-070 in Fig. 12). Oxidation of magnetite into hematite could explain this behavior.

### *Reliability of the demagnetization methods*

Abdul Aziz et al. (2008) indicated that for some samples from the eastern Bavarian Molasse sections, the AF demagnetization method does not yield reliable results. This was especially the case for samples from the PUT section, of which the AF analyzed samples had a normal direction while the TH samples were reversed. Since the OSM sediments were deposited in subaerial environments with changing (ground) water levels, goethite could have an effect on the NRM demagnetization when applying the AF method. Hence, several sister samples were selected which were first TH demagnetized at 150°C to remove miscellaneous goethite. Subsequently, the samples were AF demagnetized using the following steps: 2.5, 5, 7.5, 10, 12.5, 15, 20, 25, 30, 35, 40, 50, 60, 75, 100, 125, 150, 175, and 200 mT. The results indicate that most samples could be only demagnetized up to 50 or 60 mT (Fig. 13). At higher fields, a progressive increase in magnetic intensity occurs. Moreover, the AF demagnetization method yields poorer quality demagnetization diagrams than the TH method and remains incapable of separating overlapping magnetization directions (Fig. 13). We thus conclude that although the TH method shows a slight mineralogical instability in the temperature range between 330 and 420°C (as can be seen in Fig. 12), it is preferred over the AF

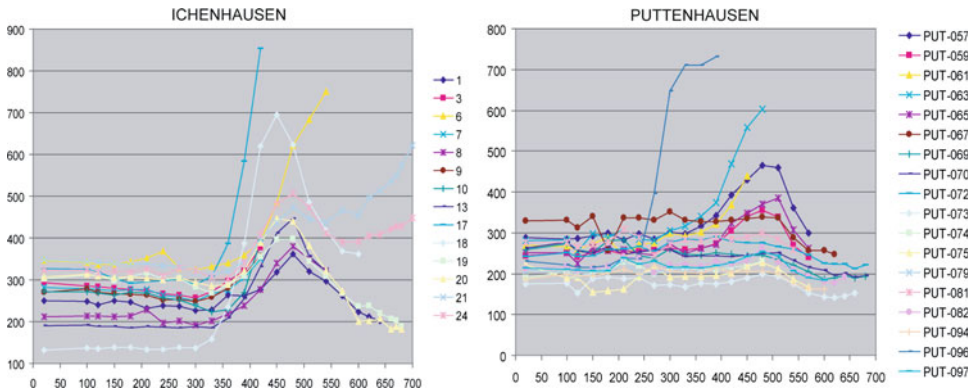


**Fig. 12** Susceptibility versus temperature measurements of selected sections and samples from the Bavarian Molasse. See text for details

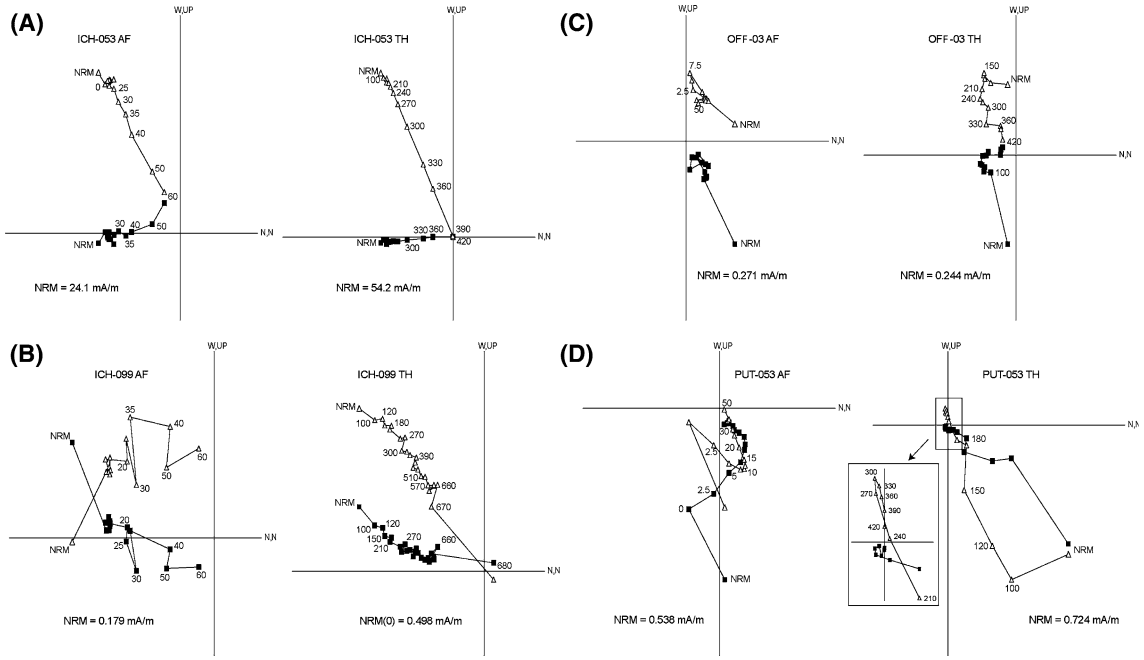


**Fig. 13** Thermal (TH) and alternating field (AF) demagnetization diagrams of selected sister samples from sections in the Bavarian Molasse. *Numbers* indicate AF steps in mT and TH steps in °C. See also caption to Fig. 11 for details

**Table 2** Mean major element composition of rhyolitic glasses from miocene bentonite horizons in the Bavarian molasse (Zahling-2, Krumbad, Hachelstuhl) and Hegau, SW-Germany (Heilsberg)

| | Zahling | | Heilsberg | | Krumbad | | Hachelstuchl | |
|---|---|---|---|---|---|---|---|---|
| | Mean | 1 sd | Mean | 1 sd | Mean | 1 sd | Mean | 1 sd |
| $SiO_2$ | 75.10 | 1.12 | 75.57 | 1.14 | 73.84 | 0.83 | 75.79 | 0.52 |
| $TiO_2$ | 0.05 | 0.03 | 0.03 | 0.03 | 0.09 | 0.03 | 0.09 | 0.03 |
| $Al_2O_3$ | 12.04 | 0.24 | 12.07 | 0.22 | 12.28 | 0.13 | 12.34 | 0.15 |
| FeO | 0.96 | 0.15 | 0.82 | 0.14 | 1.37 | 0.10 | 1.37 | 0.10 |
| MgO | 0.03 | 0.02 | 0.03 | 0.03 | 0.04 | 0.03 | 0.04 | 0.02 |
| CaO | 0.62 | 0.10 | 0.60 | 0.12 | 0.77 | 0.05 | 0.77 | 0.05 |
| MnO | 0.06 | 0.05 | 0.06 | 0.04 | 0.07 | 0.05 | 0.06 | 0.05 |
| $Na_2O$ | 2.41 | 0.31 | 2.44 | 0.32 | 2.57 | 0.33 | 2.74 | 0.53 |
| $K_2O$ | 3.51 | 0.18 | 3.22 | 0.22 | 3.27 | 0.19 | 3.69 | 0.27 |
| $P_2O_5$ | 0.02 | 0.02 | 0.01 | 0.02 | 0.02 | 0.03 | 0.01 | 0.02 |
| Total | 94.84 | 1.50 | 94.90 | 1.55 | 94.39 | 0.84 | 97.21 | 0.85 |

*1 sd* 1 standard deviation and refer to the compositional variation between individual glass shards

demagnetization method for determining the primary magnetization direction, or ChRM, in Molasse sediments.

Accordingly, the mineralogic alteration during TH demagnetization, which could be caused by the alteration of gregeite (Dr. I. Vasiliev personal communication), needs to be characterized through rock magnetic analysis combined with SEM (scanning electron microscopy) studies.

## Interpretations (Implications) and further research

### Calibration to the ATNTS04

In the article of Abdul Aziz et al. (2008), a chronostratigraphic framework for the eastern Bavarian Upper Freshwater Molasse was established by combining the magnetostratigraphy with biostratigraphic, lithostratigraphic, and $^{40}Ar/^{39}Ar$ dating results. This integrated stratigraphic approach is essential because the magnetic polarity records of the studied sections comprise none or only a few reversal levels and are thus insufficient for a direct and unambiguous magnetostratigraphic correlation to the ATNTS04 (Lourens et al. 2004). Using the same integrated approach, the new results from western Bavaria are incorporated into the established chronostratigraphic framework (Fig. 14). Abdul Aziz et al. (2008) have indicated that the magnetostratigraphic correlation of the eastern Bavarian sections to the ATNTS04 represent best-fit interpretations and that the correlation of the PUT magnetostratigraphic record could be incorrect. The new magnetostratigraphic results for the PUT section (Fig. 4), however, do not provide additional information to further confirm the proposed correlation.

With the new results of the western Bavarian sections, the chronostratigraphic framework for the Bavarian OSM is extended further into the Early Miocene. The magnetostratigraphic record of these sections are correlated to the ATNTS04 as follows (Fig. 14): the OBB section correlates

**Table 3** Summary of $^{40}Ar/^{39}Ar$ plateau and isochrone ages of bentonite-hosted rhyolitic glasses from Southern Germany

| | Zahling glass (150–200 μm) Total fusion | *N* | Zahling glass (200–250 μm) Total fusion | *N* | Zahling glass (150–250 μm) Incremental heating | *N* |
|---|---|---|---|---|---|---|
| Normal isochrone (Ma) | 16.06 ± 0.13 | 5 | 16.11 ± 0.32 | 3 | 16.12 ± 0.58 | 10 |
| Non-radiogenic $^{40}Ar/^{36}Ar$ intercept | 312.3 ± 31.2 | | 207.7 ± 121.4 | | 320.4 ± 89.9 | |
| MSWD | 1.0 4 | | 0.0 4 | | 0.5 3 | |
| Inverse isochrone (Ma) | 16.07 ± 0.13 | 5 | 16.11 ± 0.32 | 3 | 16.05 ± 0.60 | 10 |
| Non-radiogenic $^{40}Ar/^{36}Ar$ intercept | 310.9 ± 30.7 | | 209.6 ± 121.8 | | 333.4 ± 94.6 | |
| MSWD | 1.0 0 | | 0.0 4 | | 0.4 6 | |
| Weighted plateau (Ma) | 16.10 ± 0.10 | 5 | 15.89 ± 0.12 | 3 | 16.29 ± 0.14 | 10 |
| MSWD | 1.02 | | 0.57 | | 0.50 | |
| $^{39}ArK$ used in plateau calculation | 100% | | 52.5% | | 97.7% | |
| Total (Ma) | 16.12 ± 0.10 | 5 | 15.98 ± 0.11 | 5 | 16.32 ± 0.21 | 12 |
| | Krumbad glass (100–125 μm) Total fusion | *N* | Heilsberg glass (200–250 μm) Total fusion | *N* | Heilsberg K-Fp (>200 μm) Total f usion | *N* |
| Normal isochrone (Ma) | 15.62 ± 0.37 | 5 | 14.64 ± 2.73 | 4 | 14.51 ± 0.19 | 5 |
| Non-radiogenic $^{40}Ar/^{36}Ar$ intercept | 249.0 ± 94.7 | | 258.9 ± 95.9 | | 302.5 ± 39.6 | |
| MSWD | 0.8 4 | | 7.63 | | 2.2 6 | |
| Inverse isochrone (Ma) | 15.61 ± 0.37 | 5 | 14.51 ± 2.71 | 4 | 14.49 ± 0.19 | 5 |
| Non-radiogenic $^{40}Ar/^{36}Ar$ intercept | 251.7 ± 98.1 | | 264.1 ± 101.1 | | 312.0 ± 39.1 | |
| MSWD | 0.8 9 | | 7.6 8 | | 2.1 1 | |
| Weighted plateau (Ma) | 15.45 ± 0.10 | 5 | 14.62 ± 0.31 | 4 | 14.54 ± 0.14 | 5 |
| MSWD | 0.83 | | 5.84 | | 2.01 | |
| $^{39}ArK$ used in plateau calculation | 100% | | 88.6% | | 100% | |
| Total (Ma) | 15.44 ± 0.10 | 5 | 14.72 ± 0.15 | 5 | 14.54 ± 0.13 | 5 |

*N* Number of analyses used for the age calculation. Error refers 2 standard deviations

to chron C5Br, UA, and ICH sections to C5Cr and the OFF section to the normal chron C5Dn. The $^{40}Ar/^{39}Ar$ age of 15.6 Ma for the Krumbach bentonite, which corresponds lithostratigraphically to the upper yellow sandy unit of the UA section, seems to support this correlation. This also holds for the Zahling-2 glass-tuff, which corresponds to the UF lithostratigraphic unit and approximately correlates to the OBB section. The $^{40}Ar/^{39}Ar$ age of 16.1 Ma for Zahling-2 seems to corroborate the magnetostratigraphic calibration of OBB to the lower part of chron C5Br (Fig. 14).

## Pre-Riesian hiatus and minor hiatuses

As noted by Abdul Aziz et al. (2008), the proposed calibration to the ATNTS04 suggests the absence of the long reversed interval of C5Br in the sections of Bavaria, which is possibly due to a sedimentary gap called the pre-Riesian hiatus. This hiatus is attributed to tilting processes along the eastern margin of the Molasse Basin, which resulted in the erosion of a thick sedimentary sequence of OSM. Indications of a hiatus have been found in the biostratigraphic record identified by a mammal turnover (Böhme et al. 2002), which occurs throughout the basin and is contemporaneous with a stratigraphic gap between biostratigraphic units OSM C + D and OSM E (Fig. 15). According to our proposed chronostratigraphic framework, the pre-Riesian hiatus has a minimal duration of over 700 kyr in eastern Bavaria with sedimentation commencing again near the top of chron C5Br, ~15.25 Ma (Fig. 14). In the western part of the study area, the pre-Riesian hiatus is assumed to correspond to the sharp lithological transition from the blue–gray marly to the yellow sandy unit observed in the UA section (Fig. 5). However, the duration of the hiatus and subsequent onset of sedimentation in the west are difficult to assess due to a lack of suitable sections for magnetostratigraphy. Nevertheless, the biostratigraphic results of UA 565 m (Prieto et al. 2009) indicate that the hiatus has a longer duration in the East (later part of OSM E; Landshut area) and shorter in the West (early part of OSM E; Riss-Günz area). Based on the overall magnetostratigraphic calibration, we can thus infer that the pre-Riesian hiatus is younger than 16.5 Ma and

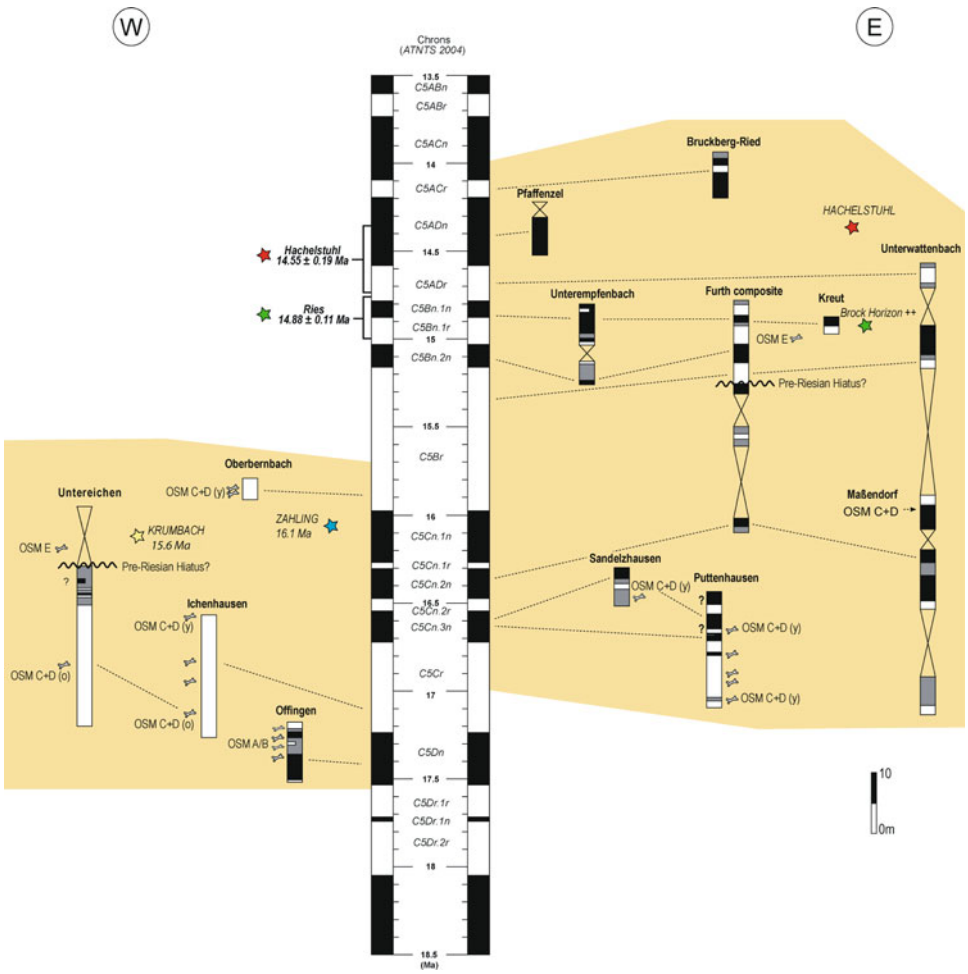


**Fig. 14** Correlation of the Bavarian magnetostratigraphic records to the Astronomical Tuned Neogene Time Scale (ATNTS) of Lourens et al. 2004. The $^{40}Ar$–$^{39}Ar$ ages of the Ries and bentonite glasses are shown with their analytical 1$\sigma$ error. Note that these ages are 0.65% older when using the Kuiper et al. 2008 intercalibrated ages of Fish Canyon Tuff. See text for details

that sedimentation in the western part of the Bavarian OSM commenced much earlier than in the eastern part, possibly between 16 and 15.5 Ma. Prieto et al. (2009) interpret the earlier onset of fluvial sedimentation in the western part, which is accompanied with a change from meandering to braided river style, as the result of Early Badenian tectonic uplift in eastern Bavaria and increased basin-wide axial slope. This induced erosion on the Landshut-Neuötting High and the eroded sediments were transported distally to the West by braided rivers.

Interestingly, in the South Bohemian České Budějovice and Třeboň Basins, a hiatus is recorded between the Early Miocene Zliv Formation and the Middle Miocene Mydlovary Formation (Hurnik and Knobloch 1966). From the lower part of the Mydlovary Formation at Strakonice, Fejfar (1974) reported a small-mammal fauna containing *Cricetodon meini*, which can thus be correlated to the late OSM E to early OSM F. Since the Mydlovary Formation also contains glass-tuffs (Hurnik and Knobloch 1966, p. 105) and is overlain by the oldest tektite-bearing sediments (reworked glasses of the Ries impact event) of the Vrábče Member (late Early Badenian according to flora, Ševčík et al. 2007) a correlation of the Mydlovary Formation with the Early Badenian Middle Series of the NAFB is reasonable. These demonstrate the presence of the pre-Riesian hiatus also in the southern part of the Bohemian Massif.

In the easternmost part of Bavaria (Lower Bavaria, region Inn-Vils), intensified tectonic tilting and uplift since the late Ottnangian result in longer sedimentation gaps and several hiatuses (Grimm 1957). The oldest one, the first Rottschwellen hiatus (Neumaier and Wieseneder 1939, Zöbelein 1940) correlate to the later part of the late Ottnangian (Fig. 15), whereas the second Rottschwellen hiatus belongs to a long sedimentation gap, which ends just in the Sarmatian with the sedimentation of the *Südlicher Vollschotter* (Grimm 1957).

In the west of the studied area, two minor hiatuses are recorded. These are the Graupensand hiatus, which was established due to the incision of the Graupensand channel (Reichenbacher et al. 1998), and in the westernmost part (west of the Iller river) the Heggbach hiatus (Fig. 15). This hiatus is identifiable at the profiles at Heggbach and Walpertshofen (Zöbelein 1983), where the lithostratigraphic unit *Fluviatile Untere Serie* lies directly on the *Albstein* (a pedogenic caliche horizon marking the top of the Upper Marine Molasse; Geyer and Gwinner 1991). About five to

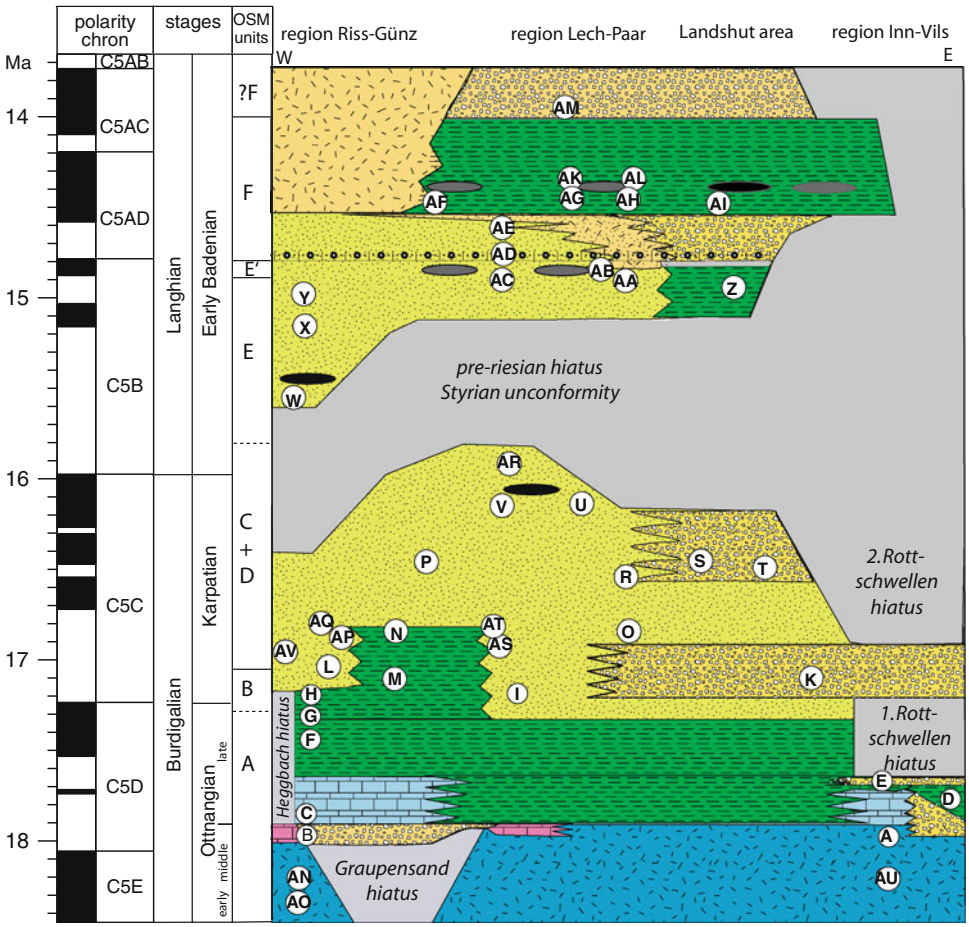


**Fig. 15** Correlation of mammal localities in the Bavarian part of the NAFB (including few localities from nearby areas, e.g., Carpatian Foredeep, Baden-Württemberg). *A* Orechov, *B* Eggingen-Mittelhart, *C* Langenau, *D* Rauscheröd, *E* Rembach, Forsthart, Hoisberg, *F* Günzburg 2, *G* Offingen 2, *H* Bellenberg 1 + 2, *I* Langenmoosen, *K* Niederaichbach, *L* Untereichen-Altenstadt 540 m, *M* Ichenhausen 3, *N* Ichenhausen 7, *O* Puttenhausen classic, *P* Burtenbach, *R* Puttenhausen E, *S* Sandelzhausen, *T* Maßendorf, *U* Affalterbach, *V* Oggenhof, *W* Untereichen-Atenstadt 565 m, *X* Mohrenhausen, Ebershausen, *Y* Edelbeuren, *Z* Furth 460 m, *AA* Unterneul 1a, *AB* Derching 1b, *AC* Ziemetshausen 1c, *AD* Ziemetshausen 1b, *AE* Ziemetshausen 1e, *AF* Thannhausen, *AG* Unterzell 1a, *AH* Laimering 2, 3, 4a, *AI* Sallmannsberg, *AK* Unterzell 1c, *AL* Laimering 4b, *AM* Laimering 5, *AN* Baltringen, *AO* Walbertsweiler, *AP* Bubenhausen, *AQ* Edelstetten, *AR* Oberbernbach, *AS* Roßhaupten, *AT* Jettingen, *AU* Auwiesholz, *AV* Heggbach. See also caption to Fig. 2 for details

ten meters above the *Albstein* a comparatively rich mammal fauna is known of which *Megacricetodon* aff. *bavaricus* is biostratigraphicaly most important (Probst 1879, Zöbelein 1983). According to Fahlbusch (in Zöbelein 1983, p. 173), this evolutionary level corresponds best to Rosshaupten, Schönenberg, and Jettingen, indicating a correlation to the early OSM C + D unit (Fig. 3). The Heggbach hiatus thus correlates to the late Ottnangian (Fig. 15).

## Chronostratigraphy

### *Ottnangian–Karpatian boundary*

The Ottnangian–Karpatian boundary is not yet defined by a boundary stratotype and therefore remains provisional (Cicha and Rögl 2003). According to the latest review of the Karpatian stage (Brzobohaty et al. 2003), this boundary is characterized solely in terms of marine biostratigraphy marked by the FAD (first appearance datum) of the benthic foraminifer *Uvigerina graciliformis* (Cicha and Rögl 2003). This event is correlated to reversal between chrons C5Cr and C5Dn (Rögl et al. 2003) and can thus be assigned an age of 17.235 Ma (Lourens et al. 2004). As the Ottnangian–Karpatian boundary interval in the Paratethys area is characterized by a far-spread regression followed by a gradual transgression (Holcova 2003), it is correlated to the beginning of the third-order TB2.2 global eustatic cycle (sensu Haq 1991, Kovac et al. 2004), which corresponds to the Bur4 sequence boundary (sensu Hardenbol et al. 1998) dated at 17.30 Ma (Wornardt 2002).

*Karpatian–Badenian boundary*

The Karpatian–Badenian boundary interval is characterized by an extensive regression followed by a transgression (beginning of the third-order TB2.3 global eustatic cycle, Kovac et al. 2004). The base of the Badenian correlates to the base of the Langhian Stage in the Mediterranean (Papp and Cicha 1978), which is usually biostratigraphically defined by the FAD of the planktonic foraminifer *Praeorbulina glomerosa* dated at 16.27 Ma (Lourens et al. 2004, but there is currently no definitive agreement about this). Actually, the base of the Langhian (and the Badenian) is provisionally placed near the *Praeorbulina* datum at the base of chron C5Cn, which is dated astronomically at 15.974 Ma (Lourens et al. 2004).

*Correlation of lithostratigraphic units to chronostratigraphy*

According to our calibration of the West-Molasse sections to the ATNTS04, the Ottnangian–Karpatian boundary correlates to the lowermost part of the *Limnische Untere Serie* (UL), defined at the top of the OFF section (Fig. 2). Since the base of the OFF section lies about 35 m above the top of the Kirchberg Formation (Brackish Water Molasse), this implies that the Brackish- to Freshwater Molasse transition already occurred during the regressive phase of the latest Ottnangian. As a consequence, the lithostratigraphic unit UL in western Bavaria corresponds to the latest Ottnangian (OFF section) and the Early Karpatian (ICH section) (Fig. 2).

The western Bavarian lithostratigraphic unit *Fluviatile Untere Serie* (UF) possibly corresponds to the Early to Late Karpatian and the Early Badenian (UA section). In eastern Bavaria, the lithostratigraphic unit *N. Vollschotter* (NV) corresponds partly to the Karpatian and partly to the Badenian (Abdul Aziz et al. 2008). The Badenian part of the NV can be subdivided into a lower part (*Zwischenmergel*—ZM) which correlates to the middle Early Badenian and an upper part (gravels with the *Sand-Mergel-Decke* including the Lower Bavarian main bentonit horizon at the top), which corresponds to the late Early Badenian (~14.8 to ~14.0 Ma). Both parts are separated by a short hiatus and the Brock-horizon.

The pre-Riesian hiatus occurred during the latest Karpatian and lower Early Badenian in Eastern Bavaria (Landshut area) and during the Late Karpatian and earliest Badenian in Western Bavaria (region Riss-Günz). According to the biostratigraphic and $^{40}Ar/^{39}Ar$ dating results, the Latest Karpatian sediments (and the Karpatian–Badenian boundary) are probably only represented in the central part of the Bavaria Molasse basin (region Lech-Paar; OBB section, Affalterbach locality, Zahling-2 glass-tuff). However, unambiguous magnetostratigraphic evidence is still missing.

*Correlation of biostratigraphic units to Chronostratigraphy*

The local OSM A correlates to the late Ottnangian (Fig. 15). Depending on the biostratigraphic position of the OFF 2 fauna (OSM A/B), the OSM B correlates either to the latest Ottnangian to earliest Karpatian, or only to the earliest Karpatian. OSM C + D correlate to the Karpatian and may also include the earliest Badenian (early part of OSM C + D to the early/middle Karpatian—ICH 3, UA 540 m; late part of OSM C + D to the late Karpatian—ICH 7, PUT A–E, Sandelzhausen faunas), and OSM E and F are correlate to the Early Badenian (Furth 460 m, UA 565 m and younger faunas; Fig. 15).

The evolutionary lineage of *Megacricetodon* (aff. *collongensis-bavaricus-lappi*) spans about three million years, from the Middle to late Ottnangian (~17.9 Ma) to the Early Badenian (~14.9 Ma). In terms of the MN- "zonation" (in the traditional sense used in the NAFB, see Heissig 1997) this implies that the MN4-MN5 "boundary" (OSM A-OSM B transition) corresponds to the Ottnangian–Karpatian boundary at 17.23 Ma (or slightly below depending on whether the OFF 2 belongs to OSM A or B), whereas the MN5-MN6 "boundary" (OSM E-OSM F transition) is of Early Badenian age around 14.8 Ma.

This new chronostratigraphic correlation of the small-mammal biostratigraphy has also implications for the chronostratigraphy of the otolith-zonation (Reichenbacher 1999). The reference locality of the assemblage zone OT-M5 is outcrop 42 g at Oberkirchberg (Reichenbacher 1993: 303), just above the Kirchberg Formation and within the lowermost Freshwater Molasse sediments, indicating that the OT-M4/OT-M5 transition is situated within the late Ottnangian.

Our biostratigraphic results suggest that the transition from the Brackish- to Freshwater Water Molasse within the NAFB occurs slightly earlier in the east (Bavaria) than in the west (Central Aargau, Switzerland), where the small-mammal fauna of Hirschthal (Kälin 1997; biostratigraphicaly indistinguishable from OFF 2 and Günzburg 2) is situated within the younger part of the Brackish Water Molasse (Kälin 1997; Fig. 2). This is in accordance with a westward directed marine regression. A subsequent short marine incursion during the early Karpatian, documented in Central Switzerland (Reichenbacher et al. 2005), is not recorded in Southern Germany and probably did not extend so far to the east.

*Mammal biostratigraphic characterization of the Ottnangian–Karpatian boundary*

The Ottnangian–Karpatian boundary is not well characterized by mammals yet (Rögl et al. 2003) and only three localities are known which directly correlate to marine Karpatian or Ottnangian sediments; Teiritzberg and Obergänserndorf, both Korneuburg Basin (Karpatian, Daxner-Höck 1998) and Orechov, Carpathian Foredeep (Ottnangian, Cicha et al. 1972, Fejfar 1974). The Orechov section is overlain by the late Ottnangian *Rzehakia*-beds, which can be correlated to the Kirchberg Formation (Reichenbacher et al. 1998). Orechov marks the FAD of *Megacricetodon* (Fejfar 1974) in Central Europe. The teeth of this population are distinctly smaller than the oldest *Megacricetodon* teeth of the NAFB from Langenau (correlative to the base of the Kirchberg Formation, Reichenbacher et al. 1998). The comparison to the fossil sites Obergänserndorf and Teiritzberg is restricted because *Megacricetodon* does not occur in the Austrian localities (Daxner-Höck 1998). However, *Microdyromys* (biostratigraphically the most important small-mammal in both localities, Daxner-Höck 1998, p. 388) may suggest a correlation to our late OSM C + D (Table 1), which agrees well with the magnetostratigraphic correlation of Obergänserndorf and Teiritzberg to chron C5Cn3n (Harzhauser et al. 2002).

The rich vertebrate record of the NAFB (15 localities between the levels of Orechov and Obergänserndorf, Teiritzberg, Fig. 15) provides for the first time enough data to characterize the Ottnangian–Karpatian time span in terms of small-mammal biostratigraphy. Using the reversal between chron C5Cr and C5Dn as the reference for this boundary (Rögl et al. 2003) the Ottnangian–Karpatian transition corresponds approximately to the transition from OSM A to OSM B. The Ottnangian–Karpatian boundary is therefore contemporaneous with the first appearance datum of *Megacricetodon bavaricus* (in the size of the type population from Langenmoosen, Fahlbusch 1964) and the first common occurrence of *Keramidomys thaleri* (appear outside the basin already during the late Ottnangian, see below), whereas *L. florancei*, *Melissiodon dominans* and *Prodeinotherium* aff. *bavaricum* have been already disappeared during the late Ottnangian (last appearance for *L. florancei* and *M. dominans* is Forsthart, Fahlbusch and Ziegler 1986; for *P.* aff. *bavaricum* Hoisberg, Grimm 1957; see Fig. 15). The FAD of *Keramidomys* probably shortly predates the boundary, since Franzensbad, the locality from the Cheb basin where the genus is first recorded (Fejfar 1974), correlates on the basis of *Megacricetodon* aff. *collongensis* with the late Ottnangian localities of the NAFB (in the NAFB *Keramidomys* first appear in the basal Karpatian of Langenmoosen, OSM B). The Ottnangian–Karpatian boundary also coincides with the beginning of the Older Series, characterized by the absence of *P. bavaricum*. The small dinotheriid proboscidian *Prodeinotherium* aff. *bavaricum* is present in late Ottnangian localities of the NAFB (Langenau, Hoisberg, see chapter biostratigraphy) and outside the basin (Franzensbad, Fejfar 1974) and is unknown in any other Karpatian site before it re-appeared in the Early Badenian Middle Series (Dehm 1951; Huttunen and Göhlich 2002). This peculiar *Prodeinotherium*-vacuum during the Karpatian of the Molasse Basin is of special biostratigraphic significance for the NAFB, and possibly for Central Europe in general.

As stated above, our results indicate that the Ottnangian–Karpatian boundary (~17.23 Ma) roughly corresponds to the MN4/5 "boundary", which is close to previous estimates of 17 Ma for this transition (Steininger 1999). However, it differs significantly from the biochronostratigraphy in Spain, where this "boundary", defined by the extinction of the genus *Ligerimys* (Daams et al. 1999a; Mein 1999), is placed at the local (Aragonian) zone C/D transition at 15.94 Ma (Daams et al. 1999b, van Dam et al. 2006). However, the biostratigraphic use of *Ligerimys* extinction is misleading since the last representatives of this genus are different in both regions. According to Alvares Sierra (1987) the last Spanish representative of *Ligerimys* is the endemic species *L. ellipticus* (characteristic for local zone C, 16.56 to 15.94 Ma), whereas *L. florancei* (the last species of the genus in Central Europe) is interpreted as an immigrant in Spain and is found only in zone B with an age between 16.88 and 16.56 Ma (Daams et al. 1999b; van Dam et al. 2006). Therefore, the presence of *L. florancei* in Central and Southwest Europe shows no overlap (~18 to ~17.6 Ma in Central Europe, 16.88 to 16.56 Ma in Spain).

*Mammal biostratigraphic characterization of the Karpatian–Badenian boundary*

Similar to the Ottnangian–Karpatian boundary, the Karpatian–Badenian boundary interval is also poorly documented by mammals. Only two localities (Grund and Mühlbach, Daxner-Hoeck 2003) are known in the Central Paratethys that could be directly correlated to marine Early Badenian sediments, however, these localities are significantly younger than the Karpatian–Badenian boundary. Both localities belong to the upper part of Lower Lagenid zone (late M5b-M6, ~15.1 Ma; Rögl et al. 2002; Rögl and Spezzaferri 2003; Ćorić et al. 2004) and correlate to the late OSM E (Prieto et al. 2009). A problem to characterize the boundary is that in most circum alpine basins this period is represented by hiatuses (Rögl et al. 2002). In the Bavarian part of the NAFB, the boundary will be probably crossed only in the central part (NE of Augsburg, Lech region, Fig. 3), from which the biostratigraphic data are poor at the moment (see biostratigraphic results from the OBB section). The youngest biostratigaphically well-dated late Karpatian locality is Affalterbach (Prieto and Böhme 2007; Prieto

2009). Except the unusual glirid *Seorsumuscardinus bolligeri* the small-mammals of Affalterbach correspond to other faunas from the late OSM C + D and early OSM E. The most characteristic event during the earliest Badenian is the significant size increase in the large *Megacricetodon* lineage (Fig. 3). Large mammal events like the re-immigration of *Prodeinotherium* and the FAD of *Pliopithecus* also occurred in the early Badenian before 15 Ma, however the exact time constraint remains obscure.

### *Use of volcanic ash horizons and sedimentary cycles for regional lithotratigraphic correlation*

According to our field studies and $^{40}Ar/^{39}Ar$ results, at least four stratigraphically different volcanic ash horizons can be distinguished in the Bavarian part of the NAFB. These horizons include the glass-tuffs at Zahling-2 (16.1 Ma) and Krumbad (15.6 Ma), the bentonite at Unterneul (not measured here; just below the Ries boulders, Fiest 1989, ~14.9 Ma) and the Hachelstul and Hegau glass-tuffs (14.5 Ma). Except for the Unterneul bentonite (also known from Oberschöneberg, Schmid 2002), which is completely lacking residual glass and characterized by large biotite crystals, all other glass-tuffs and bentonites are petrographically, geochemically, and isotopically similar (this study and Ulbig 1994). Therefore, non-dated volcanic ash layers and bentonites are unreliable stratigraphic tools for regional or basin-wide correlations in the NAFB.

Similarly, our field work suggests that sedimentary cyclicity (see Heissig 1997) although useful on local scale (Fiest 1989), and as for the *N. Vollschotter* in the Landshut area even recognizable over tens of kilometers (Abdul Aziz et al. 2008), is not appropriate for correlation on a regional or basin-wide scale.

**Acknowledgments** We thank Harald Schmidt (Tonwerk Ichenhausen), Wolfgang Neumann (Ziegelwerk Bellenberg), and Georg Bauer (Ziegelwerke Leipfinger-Bader, Puttenhausen) for working permissions and technical help in the clay pits. Special thanks to Gerhard Doppler (Bavarian Geological Survey), Bettina Reichenbacher (LMU Munich), and Jean-Pierre Berger (University Fribourg) for fruitful discussions about the geology and stratigraphy of the West-Molasse and helpful comments on the manuscript. This project was supported by DFG grants BO 1550/7-1, 2 and BO 1550/8.

## Appendix

See Appendix Table 4 and Fig. 16

**Table 4** $^{40}Ar/^{39}Ar$ plateau ages and $^{39}Ar/^{37}Ar$-derived K/Ca ratios of rhyolitic bentonite-hosted glasses from Southern Germany

| | Plateau Age [Ma] | 2s | K/Ca | 2s | | Plateau Age [Ma] | 2s | K/Ca | 2s |
|---|---|---|---|---|---|---|---|---|---|
| *Zahling (150-200μm glass fragments, total fusion)* | | | | | *Krumbach (100-125μm glass fragments, total fusion)* | | | | |
| Zah-01 | 16.14 | 0.10 | 6.618 | 0.388 | Kru-01 | 15.47 | 0.10 | 4.443 | 0.236 |
| Zah-02 | 16.09 | 0.11 | 6.799 | 0.428 | Kru-02 | 15.41 | 0.11 | 4.346 | 0.236 |
| Zah-03 | 16.11 | 0.08 | 6.998 | 0.414 | Kru-03 | 15.51 | 0.16 | 4.394 | 0.264 |
| Zah-04 | 16.04 | 0.08 | 6.700 | 0.460 | Kru-04 | 15.48 | 0.08 | 4.430 | 0.231 |
| Zah-05 | 16.14 | 0.09 | 6.682 | 0.356 | Kru-05 | 15.39 | 0.10 | 4.492 | 0.244 |
| *Zahling (200-250μm glass fragments, total fusion)* | | | | | *Heilsberg (200-250μm glass fragments, total fusion)* | | | | |
| Zah-06 | 15.84 | 0.14 | 6.957 | 0.476 | Hb-2a-01 | 14.08 | 0.34 | 6.132 | 0.488 |
| Zah-07 | 15.90 | 0.12 | 6.657 | 0.357 | Hb-2a-02 | 14.45 | 0.25 | 5.941 | 0.398 |
| Zah-08 | 15.93 | 0.12 | 6.914 | 0.410 | Hb-2a-03 | 14.77 | 0.17 | 5.696 | 0.348 |
| Zah-09 | 16.06 | 0.08 | 6.378 | 0.338 | Hb-2a-04 | 14.89 | 0.33 | 5.736 | 0.412 |
| Zah-10 | 16.08 | 0.12 | 6.759 | 0.398 | Hb-2a-05[a] | 15.73 | 0.34 | 5.639 | 0.454 |
| *Zahling (150-200μm glass fragments, incremental heating)* | | | | | *Heilsberg (alkali feldspar, total fusion)* | | | | |
| Zah-10[a] | 20.53 | 36.9 | - | - | Hb-2a-06 | 14.36 | 0.26 | 0.407 | 0.021 |
| Zah-11[a] | 19.16 | 3.44 | 0.937 | 0.358 | Hb-2a-07 | 14.52 | 0.10 | 0.505 | 0.026 |
| Zah-12 | 15.62 | 1.55 | 2.521 | 1.163 | Hb-2a-08 | 14.45 | 0.22 | 0.215 | 0.011 |
| Zah-13 | 16.08 | 0.64 | 2.807 | 0.978 | Hb-2a-09 | 14.72 | 0.28 | 0.236 | 0.012 |
| Zah-14 | 16.53 | 0.63 | 3.069 | 1.166 | Hb-2a-10 | 14.77 | 0.24 | 0.295 | 0.015 |
| Zah-15 | 16.32 | 0.34 | 4.000 | 2.182 | | | | | |
| Zah-16 | 16.34 | 0.29 | 3.470 | 1.045 | | | | | |
| Zah-17 | 16.11 | 0.46 | 3.032 | 1.430 | | | | | |
| Zah-18 | 16.20 | 0.19 | 4.311 | 2.143 | | | | | |
| Zah-19 | 16.33 | 0.17 | 2.612 | 1.099 | | | | | |
| Zah-20 | 16.47 | 0.41 | 2.347 | 1.271 | | | | | |
| Zah-21 | 16.14 | 0.85 | 1.126 | 0.891 | | | | | |

*2s* 2 standard deviation

[a] Data regarded as outliers and not used for age calculation

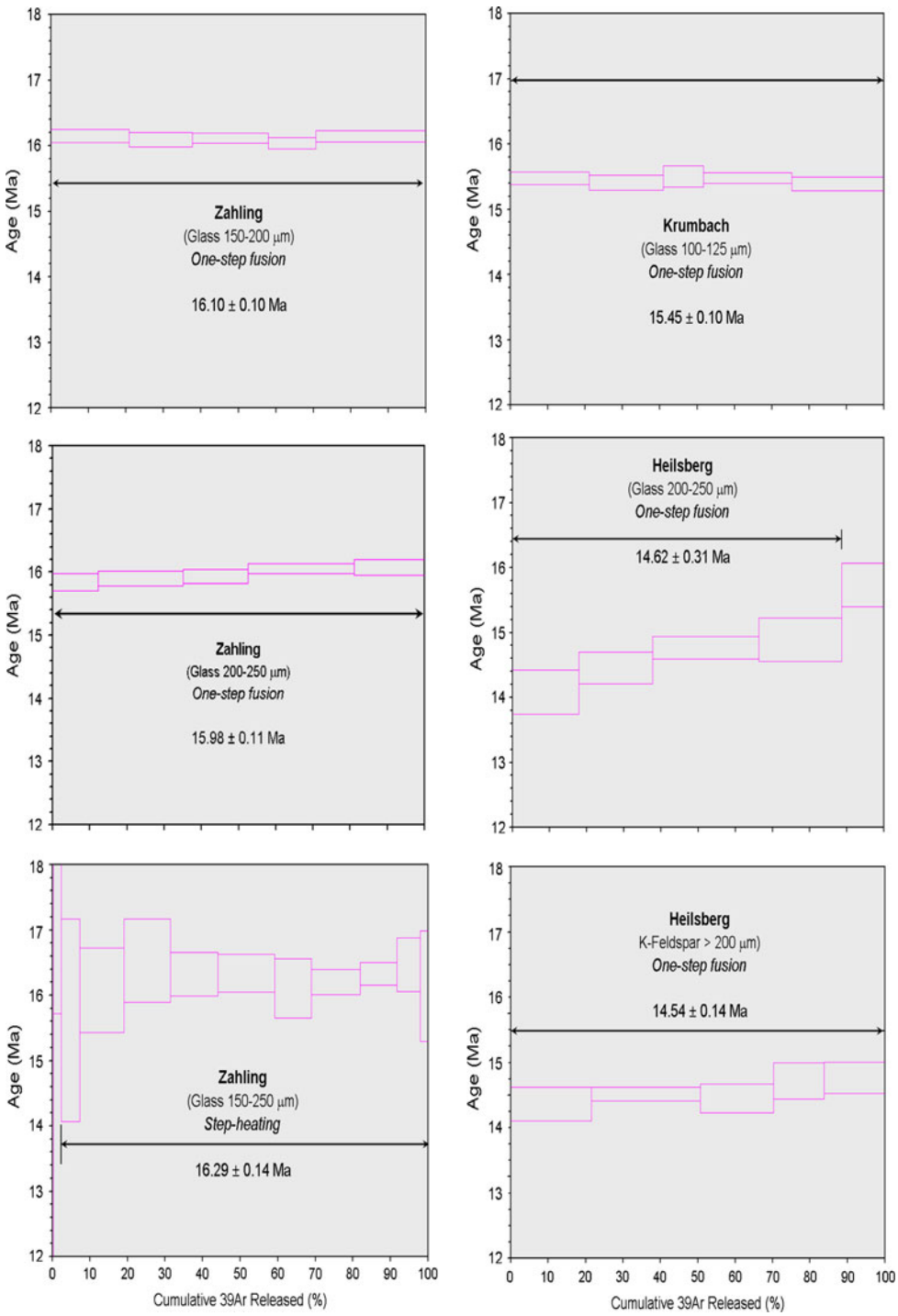


**Fig. 16** Weighted mean plateau ages of total fusion and incremental heating experiments for bentonite-hosted rhyolitic glasses from Southern Germany. Plateau steps and their $1\sigma$-error are shown. Total procedure blanks ranged from $1.2 \times 10^{-3}$ to $3.8 \times 10^{-3}$ V for mass 36, $1.0 \times 10^{-3}$ to $3.2 \times 10^{-3}$ V for mass 37, $0.2 \times 10^{-4}$ to $13 \times 10^{-4}$ V for mass 38, $0.6 \times 10^{-4}$ to $3.1 \times 10^{-4}$ V for mass 39, and $2.3 \times 10^{-2}$ to $4.8 \times 10^{-2}$ V for mass 40, based on a system sensitivity of $1.8 \times 10^{-17}$ mol/V

## References


Abdul Aziz H, Böhme M, Rocholl A, Zwing A, Prieto J, Wijbrans JR, Heissig K, Bachtadse V (2008) Integrated stratigraphy and $^{39}Ar/^{40}Ar$ dating of the early to middle miocene upper freshwater molasse in eastern Bavaria (Germany). Int J Earth Sci 97:115–134

Alvares Sierra MA (1987) Estudio sistemático y biostratigráphico de los Eomyidae (Rodentia) del Oligocene superior y Mioceno inferior espanol. Scripta Geologica 86:207

Batsche H (1957) Geologische Untersuchungen in der Oberen Süßwassermolasse Ostniederbayerns (Blatt Landau, Eichendorf, Simbach, Arnstorf der Topogr. Karte 1:25 000). Beihefte zum Geologischen Jahrbuch 26:261–307

Berger J-P (1999) Redefinition of European oligo-miocene charophyte biozonation. Aust J Bot 47(3):283–296

Böhme M, Gregor H-J, Heissig K (2002) The Ries- and Steinheim meteorite impacts and their effect on environmental conditions in time and space. In: Buffetaut E, Koerbel C (eds) Geological and biological effects of impact events. Springer, Berlin, pp 215–235

Bolliger T (1992) Kleinsäugerstratigraphie in der miozänen Hörnlischüttung (Ostschweiz). Documenta Naturae 75:1–296

Boon E (1991) Die Cricetiden und Sciuriden der Oberen Süßwasser-Molasse von Bayerisch-Schwaben und ihre stratigraphische Bedeutung. PhD-thesis, LMU Munich, 159 pp

Brzobohaty R, Cicha I, Kovac M, Rögl F (eds) (2003) The Karpatian—A lower miocene stage of the central Paratethys. Masaryk University, Bratislava, p 360

Buchner E, Seyfried H, van den Bogaard P (2003) $^{40}Ar/^{39}Ar$ laser probe age determination confirms the Ries impact crater as the source of glass particles in Graupensand sediments (Grimmelfingen Formation, North Alpine Foreland Basin). Int J Earth Sci 92:1–6

Cicha I, Rögl F (2003) Definition of the Karpatian stage. In: Brzobohaty R, Cicha I, Kovac M, Rögl F (eds) The Karpatian—A lower miocene stage f the central Paratethys. Masaryk University, Bratislava, pp 15–20

Cicha I, Fahlbusch V, Fejfar O (1972) Die biostratigraphische Korrelation einiger jungtertiärer Wirbeltierfaunen Mitteleuropas. Neues Jahrbuch für Geologie und Paläontologie. Abhandlungen 140(2):129–145

Ćorić S, Harzhauser M, Hohenegger J, Mandic O, Pervesler P, Roetzel R, Rögl F, Spezzaferri S, Stingl K, Svábenická L, Zorn I, Zuschin M (2004) Stratigraphy and correlation of the grund formation in the molasse basin, northeastern Austria (Middle Miocene, Lower Badenian). Geologica Carpathica 55:207–215

Daams R, van der Meulen A, Alvarez Sierra MA, Peláez-Campomanes P, Krijgsman W (1999a) Aragonian stratigraphy reconsidered, and a re-evaluation of the middle miocene mammal biochronology in Europe. Earth Planet Sci Lett 165:287–294

Daams R, van der Meulen A, Alvarez Sierra MA, Peláez-Campomanes P, Calvo JP, Alonso Zarza MA, Krijgsman W (1999b) Stratigraphy and sedimentology of the Aragonian (Early to Middle Miocene) in its type area (North-Central Spain). Newsl Stratigr 37(3):103–139

Dam van J, Abdul Aziz H, Álvarez Sierra MA, Hilgen FJ, van den Hoek Ostende LW, Lourens LJ, Mein P, van der Meulen AJ, Pelaez-Campomanes P (2006) Long-period astronomical forcing of mammal turnover. Nature 443(12):687–691

Daxner-Höck G (1998) Säugetiere (Mammalia) aus dem Karpat des Korneuburger Beckens. 3. Rodentia und Carnivora. Beiträge zur Paläontologie 23:367–407

Daxner-Hoeck G (2003) Mammals from the Karpatian of the central Paratethys. In: Brzobohaty R, Cicha I, Kovac M, Rögl F (eds) The Karpatian–a Lower Miocene stage of the Central Paratethys. Masaryk University, Bratislava, pp 293–310

Dehm R (1951) Zur Gliederung der jungtertiären molasse in Süddeutschland nach Säugetieren. Neues Jahrbuch für Geologie und Paläontologie, Monatshefte, pp 140–152

Dehm R (1955) Die Säugetierfaunen der Oberen Süßwassermolasse und ihre Bedeutung für die Gliederung. In: Bayerisches Geologisches Landesamt (eds) Erläuterungen zur Geologischen Übersichtskarte der Süddeutschen Molasse. Bayerisches Geologisches Landesamt, Munich, pp 81–87

Doppler G (1989) Zur Stratigraphie der nördlichen Vorlandmolasse in Bayerisch-Schwaben. Geol Bavarica 94:83–133

Doppler G, Heissig K, Reichenbacher B (2005) Die Gliederung des Tertiärs im süddeutschen Molassebecken. Newsl Stratigr 41:359–375

Engelhardt Wv (1956) Neuere Untersuchungen über den Hegau-Vulkanismus. Jahresbericht und Mitteilungen des oberrheinischen geologischen Vereins N.F. 47:79–90

Fahlbusch V (1964) Die Cricetiden (Mamm.) der Oberen Süßwassermolasse. Bayerische Akademie der Wissenschaften, math.-naturw.-Kl., Abh., N.F. 118, 136 pp

Fahlbusch V, Wu W (1981) Puttenhausen: Eine neue Kleinsäuger-Fauna aus der oberen Süßwasser-Molasse Niederbayerns. Mitteilungen der Bayerischen Staatssammlung für Paläontologie und historische Geologie 21:115–119

Fahlbusch V, Ziegler R (1986) Kleinsäuger-Faunen aus der basalen Oberen Süßwasser-Molasse Niederbayerns. Zitteliana 14:3–80

Fejfar O (1974) Die Eomyiden und Cricetiden (Rodentia, Mammalia) des Miozäns der Tschechoslovakei. Paleontographica (A) 146: 99–180

Fiest W (1989) Lithostratigraphie und Schwermineralgehalt der Mittleren und Jüngeren Serie der Oberen Süßwassermolasse Bayerns im Übergangsbereich zwischen Ost- und Westmolasse. Geol Bavarica 94:259–279

Gentner W, Lippolt HJ, Schaefer OA (1963) Argonbestimmungen an Kaliummineralien–XI Die Kalium-Argon-Alter der Gläser des Nördlinger Rieses und der böhmisch-mährischen Tektite. Geochimica et Cosmochimica Acta 27(2):191–200

Geyer OF, Gwinner MP (1991) Geologie von Baden-Württemberg E. Schweizerbart, Stuttgart, p 472

Gilg AH (2005) Eine geochemische Studie an Bentoniten und vulkanischen Gläsern des nordalpinen Molassebeckens (Deutschland, Schweiz). Annual Meeting DTTM (Deutsche Ton- und Tonmineralgruppe)11, p 17

Grimm W-D (1957) Stratigraphische und sedimentpetrographische Untersuchungen in der Oberen Süßwassermolasse zwischen Inn und Rott (Niederbayern). Beih Geol Jb 26:97–199

Gubler T, Meier M, Oberli F (1992) Bentonites as time markers for sedimentation of the upper freshwater Molasse: geological observations corroborated by high-resolution single-Zircon U-Pb ages. 172. Jahresversammlung der SANW, pp 12–13

Haq BU (1991) Sequence stratigraphy, ea level change and significance for the deep sea. Spec Publ Int Ass Sediment 12:3–39

Hardenbol J, Thierry J, Farley MB, Jacquin T, de Graciansky PC, Vail PR (1998) Mesozoic and cenozoic sequence chronostratigraphic framework of European basins. In: de Graciansky PC, Hardenbol J, Jacquin T, Vail PR (eds) Mesozoic and cenozoic sequence stratigraphy of European basins. SEPM Special Publications 60, pp 3–13

Harr K (1976) Mineralogisch-petrographische Untersuchungen an Bentoniten in der Süddeutschen Molasse. PhD thesis, University Tübingen, 135 pp

Harzhauser M, Böhme M, Mandic O, Hofmann C (2002) The Karpatian (Late Burdigalian) of the Korneuburg basin. A palaeoecological and biostratigraphical synthesis. Beiträge zur Paläontologie 27:441–456

Heissig K (1997) Mammal faunas intermediate between the reference faunas of MN4 and MN6 from the upper freshwater molasse of Bavaria. In: Aguilar JP, Legendre S, Michaux J (eds) Actes du Congres BiochroM'97. Mem Trav EPHE, Inst Montpellier, vol 21. pp 537–546

Heissig K (2006) Biostratigraphy of the "main bentonite horizon"of the upper freshwater molasse in Bavaria. Palaeontographica A 277:93–102

Heizmann E (1984) *Deinotherium* im Untermiozän von Langenau und seine Bedeutung für die Untergliederung der Molasse. Molasseforschung 84—zum Gedenken an August Wetzler (1812–1881), Historischer Verein Günzburg, pp 36–39

Hofmann F (1951) Zur Stratigraphie und Tektonik des st.gallisch-thurgauischen Miozäns (Obere Süßwassermolasse) und zur Bodenseegeologie. PhD thesis, University Zürich, pp 88, Zollikofer & Co. Buchdruckerei St. Gallen

Hofmann F (1956) Sedimentpetrographische und tonmineralogische Untersuchungen an Bentoniten der Schweiz und Südwestdeutschlands. Eclogae Geologicae Helvetiae 49(1): 113–133

Hofmann B (1973) Erläuterungen zur Geologische Karte von Bayern 1:25,000 Blatt Nr. 7439 Landshut Ost. Bayerisches Geologisches Landesamt, 113 pp

Holcova K (2003) The Ottnangian/Karpatian boundary interval in Slovak neogene basins. In: Brzobohaty R, Cicha I, Kovac M, Rögl F (eds) The Karpatian—a lower miocene stage f the central Paratethys. Masaryk University, Bratislava, pp 123–126

Homewood P, Allen PA, Williams GD (1986) Dynamics of the molasse basin of western Switzerland. In: Allen PA, Homewood P (eds) Foreland basins. Special Publication of International Association of Sedimentologists, vol 8. Blackwell, Oxford, pp 199–217

Hurnik S, Knobloch E (1966) Einige Ergebnisse paläontologischer und stratigraphischer Untersuchungen im Tertiär Böhmens. Abhandlungen Staatliches Museum Mineralogie Geologie Dresden 11:17–161

Huttunen K, Göhlich UB (2002) A partial skeleton of *Prodeinotherium bavaricum* (Proboscidea, Mammalia) from the middle miocene of Unterzolling (Upper Freshwater Molasse, Germany). Geobios 35:489–514

Kälin D (1997) The mammal zonation of the upper marine molasse of Switzerland reconsidered—A local biozonation of MN2–MN5. In: Aguilar JP, Legendre S, Michaux J (eds) Actes du Congres BiochroM'97. Mem Trav EPHE, Inst Montpellier, vol 21. pp 515–536

Kempf O, Bolliger T, Kälin D, Engesser B, Matter A (1997) New magnetostratigraphic calibration of early to middle miocene mammal biozones of the North Alpine foreland basin. In: Aguilar J-P, Legendre S, Michaux J (eds) Actes du Congrès BiochroM'97. Mém Trav EPHE, Inst Montpellier, vol 21. pp 547–561

Kempf O, Matter A, Burbank W, Mange M (1999) Depositional and structural evolution of a foreland basin margin in a magnetostratigraphic framework: the eastern Swiss molasse basin. Int J Earth Sci 88:253–275

Kirschvink JL (1980) The least square line and plane and the analysis of paleomagnetic data. Geophys J Royal Astron Soc 62:699–718

Kovac M, Barath I, Harzhauser M, Hlavaty I, Hudackova N (2004) Miocene depositional systems and sequence stratigraphy of the Vienna basin. Courier Forsch-Inst Senckenberg 246:187–212

Kraus MJ, Aslan A (1993) Eocene hydromorphic paleosols: significance for interpreting ancient floodplain processes. J Sed Petrol 63:453–463

Kuhlemann J, Kempf O (2002) Post-Eocene evolution of the north Alpine foreland basin and its response to Alpine tectonics. Sediment Geol 152:45–78

Kuhlemann J, Frisch W, Székely B, Dunkl I, Kázmér M (2002) Post-collisional sediment budget history of the Alps: tectonic versus climatic control. Int J Earth Sci 91:818–837

Kuiper KF, Deino A, Hilgen FJ, Krijgsman W, Renne PR, Wijbrans JR (2008) Synchronizing rock clocks of earth history. Science 320:500–504

Lippolt HJ, Gentner W, Wimmenauer W (1963) Altersbestimmung nach der Kalium-Argon-Methode an tertiären Eruptivgesteinen Südwestdeutschlands. Jahresheft des Geologischen Landesamtes in Baden-Württemberg 6:507–538

Lourens LJ, Hilgen FJ, Laskar J, Shackleton NJ, Wilson D (2004) The neogene period. In: Gradstein FM, Ogg JG, Smith AG (eds) Geologic time scale 2004. Cambridge, Cambridge University Press, pp 409–440

Maurer H, Buchner E (2007) Rekonstruktion fluvialer Architekturelemente mäandrierender Flusssysteme mittels Paläoböden (Obere Süßwassermolasse, Nordalpines Vorlandbecken, SW-Deutschland). Zeitschrift der Deutschen Gesellschaft für Geowissenschaften 158(2):271–285

Mein P (1999) European miocene mammal biochronology. In: Rössner GE, Heissig K (eds) The miocene land mammals of Europe. Verlag Dr. Friedrich Pfeil, München, pp 25–38

Neumaier F, Wieseneder H (1939) Geologische und sedimentpetrographische Untersuchungen im Niederbayerischen Tertiär—Blatt Griesbach und Birnbach. Sitzungsberichte Bayerische Akademie der Wissenschaften, math.-naturw.-Kl. 1939, pp 177–252

Papp A, Cicha I (1978) Definition der Zeiteinheit M4—Badenien. In: Papp A, Cicha I, Senes J, Steininger F (eds) M4 Badenien (Moravien, Wielicien, Kosovien). Chronostratigraphie Neostratotypen 6, Bratislava, 594 pp

Pippèrr M, Reichenbacher B, Witt W, Rocholl A (2007) The middle and upper Ottnangian of the Simssee area (SE Germany): micropalaeontology, biostratigraphy and chronostratigraphy. Neues Jahrbuch Geologie Paläontologie Abhandlungen 245(3):353–378

Prieto J (2009) Comparison of the dormice (Gliridae, Mammalia) *Seorsumuscardinus alpinus* Bruijn, 1998 and *Heissigia bolligeri* Prieto, Böhme, 2007. Neues Jahrbuch für Geologie und Paläontologie, Abhandlungen 252(3):377

Prieto J, Böhme M (2007) *Heissigia bolligeri* gen. et sp. nov.: a new enigmatic dormouse (Gliridae, Rodentia) from the miocene of the Northern Alpine foreland basin. Neues Jahrbuch für Geologie und Paläontologie, Abhandlungen 245(3):301–307

Prieto J, Böhme M, Maurer H, Heissig K, Abdul-Aziz H (2009) Sedimentology, biostratigraphy and environments of the Untere Fluviatile Serie (Lower and Middle Miocene) in the central part of the north Alpine foreland basin—Implications for basin evolution. Int J Earth Sci. doi:10.1007/s00531-008-0331-2 (in press)

Probst J (1879) Verzeichnis der Fauna und Flora der Molasse im Württembergischen Oberschwaben. Jahreshefte Vereins vaterländische Naturkunde Württemberg 35:221–304

Reichenbacher B (1989) Feinstratigraphische Gliederung der Kirchberger Schichten (Unter Miozän) an der Typelokalität Illerkirchberg bei Ulm. Geol Bavarica 94:135–177

Reichenbacher B (1993) Mikrofaunen, Paläogeographie und Biostratigraphie der miozänen Brack- und Süßwassermolasse in der westlichen Paratethys unter besonderer Berücksichtigung der Fisch-Otolithen. Senckenbergiana lethaea 73(2):277–374

Reichenbacher B (1999) Preliminary otolith-zonation in continental Tertiary deposits of the Paratethys and adjacent areas. Neues Jahrbuch Geologie Paläontologie Abhandlungen 214(3):375–390

Reichenbacher B, Böttcher R, Bracher H, Doppler G, von Engelhardt W, Gregor H-J, Heissig K, Heizmann EPJ, Hofmann F, Kälin D, Lemke K, Luterbacher H, Martini E, Pfeil F, Reiff W, Schreiner A, Steininger FF (1998) Graupensandrinne-Ries-Impakt: Zur Stratigraphie der Grimmelfinger Schichten, Kirchberger Schichten und Oberen Süßwassermolasse. Z dt geol Ges 149:127–161

Reichenbacher B, Kälin D, Jost J (2005) A fourth St. Gallen formation cycle (?) in the Karpatian upper marine molasse of central Switzerland. Facies 51:160–172

Renne PR, Swisher CC III, Deino AL, Karner DB, Owens TL, DePaolo DJ (1998) Intercalibration of standards, absolute ages and uncertainties in $^{40}Ar/^{39}Ar$ dating. Chem Geol 145:117–152

Rocholl A, Böhme M, Guenther R, Höfer H, Ulbig A (2008) Prevailing stratospheric easterly wind direction in the Paratethys during the lower Badenian: Ar–Ar- and Nd-isotopic evidence from rhyolitic ash layers in the upper freshwater molasse, S-Germany. Geophysical Research Abstracts 10, EGU2008-A-08747, SRef-ID: 1607-7962/gra/EGU2008-A-08747

Rögl F, Spezzaferri S (2003) Foraminiferal paleoecology and biostratigrphy of the Mühlbach section (Gaindorf Formation, Lower Badenian). Annalen des Naturhistorischen Museums Wien 104A:23–75

Rögl F, Spezzaferri S, Ćorić S (2002) Micropaleontology and biostratigraphy of the Karpatian–Badenian transition (Early–Middle Miocene boundary) in Austria (Central Paratethys). Courier Forschungsinstitut Senckenberg 237:47–67

Rögl F, Ćorić S, Daxner-Höck G, Harzhauser M, Mandic O, Švábenická L, Zorn I (2003) Correlation of the Karpatian stage. In: Brzobohaty R, Cicha I, Kovac M, Rögl F (eds) The Karpatian—A lower miocene stage of the central Paratethys. Masaryk University, Bratislava, pp 27–34

Scheuenpflug L (1980) Neue Funde ortsfremder Weißjurageseine in Horizonten der südbayerischen miozänen Oberen Süßwassermolasse um Augsburg. Jber Mitt oberrhein-geol Ver NF 62:131–142

Schlunegger F, Burbank DW, Matter A, Engesser B, Mödden C (1996) Magnetostratigraphic calibration of the Oligocene to middle miocene (30–15 Ma) mammal biozones and depositional sequences of the Swiss molasse basin. Eclogae Geol Helv 89:753–788

Schlunegger F, Jordan TE, Klaper EM (1997) Controls of erosional denudation in the orogen on foreland basin evolution: the Oligocene central Swiss molasse basin as an example. Tectonics 16:823–840

Schlunegger F, Melzer J, Tucker GE (2002) Climate, exposed source rock lithologies, crustal uplift and surface erosion: a theoretical analysis calibrated with data from the Alps/North Alpine Foreland Basin system. Int J Earth Sci 90:484–499

Schmid W (1994) Lithofazielle Untersuchungen im tertiären Hügelland nördlich von Dasing. Unpublished Diploma thesis, LMU München, 164 pp

Schmid W (2002) Ablagerungsmilieu, Verwitterung und Paläoböden feinklastischer Sedimente der Oberen Süßwassermolasse Bayerns. Bayerische Akademie der Wissenschaften, math.-naturw.-Kl., Abh., N.F. 172, 247 pp

Schötz M (1993) Zwei Hamsterfaunen (Rodentia, Mammalia) aus der Niederbayerischen Molasse. Mitteilungen der Bayerischen Staatssammlung für Paläontologie und historische Geologie 33:155–194

Ševčík J, Kvaček Z, Mai H-D (2007) A new masixioid florula from the tektite-bearing deposits in south Bohemia, Czech Republic (Middle Miocene, Vrábče Member). Bull Geosci 82(4):429–436

Steininger FF (1999) Chronostratigraphy, geochronology and biochronology of the miocene "European Land Mammal Mega-Zones" (ELMMZ) and the miocene "Mammal-Zones (MN-Zones)". In: Rössner GE, Heissig K (eds) The miocene land mammals of Europe. Verlag Dr Friedrich Pfeil, München, pp 9–24

Storzer D, Gentner W (1970) Spaltspuren-Alter von Riesgläsern, Moldaviten und Bentoniten. Jahresbericht Mitteilungen Oberrheinischen Geologischen Vereins 52:97–111

Storzer D, Jessberger EK, Kunz J, Lange J-M (1995) Synopsis von Spaltspuren- und Kalium-Argon-Datierungen an Ries-Impaktgläsern und Moldaviten. In: Abstract, 4th Annual Meeting of the Gesellschaft für Geowissenschaften, vol 195. pp 79–80

Ulbig A (1994) Vergleichende Untersuchungen an Bentoniten, Tuffen und sandig-tonigen Einschaltungen in den Bentonitlagerstätten der Oberen Süßwassermolasse Bayerns. unveröff. Dissertation TU München, 245 S, München

Wijbrans JR, Pringle MS, Koppers AAP, Scheveers R (1995) Argon geochronology of small samples using the Vulkaan argon laserprobe. Proceedings Kon Ned Akad Wetensch 98(2):185–218

Wornardt WW (2002) Ages of maximum flooding surfaces and revisions of sequence boundaries and their ages, cenozoic to triassic. source: www.micro-strat.com/14072PAPER.PDF) 18 pp, Offshore Technology Conference

Wurm A (1937) Beiträge zur Kenntnis der nordalpinen Saumtiefe zwischen unterem Inn und unterer Isar. Neues Jahrbuch Mineralogie etc Beil-Bd 78 B:285–326

Ziegler R (1995) Die untermiozänen Kleinsäugerfaunen aus den Süßwasserkalken von Engelswies und Schellenfeld bei Sigmaringen (Baden-Württemberg). Stuttgarter Beiträge zur Naturkunde B 228, 53 pp

Zijderveld JDA (1967) A.C. demagnetization of rocks: analysis of results. In: Collinson et al (eds) Methods in paleomagnetizm. Elsevier, Amsterdam, pp 254–286

Zöbelein HK (1940) Geologische und sedimentpetrographische Untersuchungenim niederbayerischen Tertiär (Blatt Pfarrkirchen). Neues Jahrbuch Mineralogie Geologie Paläontologie 84 B:233–302

Zöbelein HK (1983) Die Vorlandmolasse bei Günzburg a. d. Donau und Heggbach bei Biberach a. d. Riß im Rahmen des süddeutschen Jungtertiärs. Mitteilungen der Bayerischen Staatssammlung für Paläontologie und historische Geologie 23:151–187